**Modulating Porous Carbon Electrocatalyst for Efficient Water Splitting**

**A thesis submitted in fulfilment of the requirements for the degree of**

**Master of Philosophy**

**Of The University of Sydney by**

**Yaojie Lei**


**The School of Chemical and Biomolecular Engineering**

**August 2017**

# Declaration

I declare this thesis is to the best of my own knowledge, the entire work has not been submitted previously for any other degree.

Yaojie Lei

Sep. 2017

**Abstract**

The increasing public issues about the energy crisis urge the development of sustainable energy as alternatives to replace the fossil fuels. Considering the energy regeneration and environment friendly, hydrogen possesses the potential to meet the criterion of renewable and clean energies. $H_2$ can be produced in an electrochemical water electrolyser by cathodic hydrogen evolution reaction (HER), coupled with anodic oxygen evolution reaction (OER). The kinetic barrier of both reactions require efficient electrocatalysts. However, the benchmarking electrocatalysts for HER or OER are based on precious metals, such as Pt or Ir, their high cost greatly hinders the practical $H_2$ production from water electrolyser in an economic manner. Thus, the search of in-expensive but efficient HER and OER electrocatalysts is imminent.

Among various candidature materials, low cost and high conductive carbon based nanomaterials have attracted intensive attention. Through heteroatom doping, the inert carbon nanomaterials can be activated to show promising catalytic activity. In this study, nitrogen doped nanoporous carbon electrocatalysts were obtained from thermal pyrolysis of a zinc based metal-organic framework. Cathodic treatment is successfully applied to achieve systematic modulation of the type and surface functionalities. The modulated electrocatalysts show high activity and good stability towards hydrogen and oxygen evolution in various electrolyte. Strong correlation between catalytic performance and surface chemical properties of these carbon electrocatalysts has been found. My work here paves a new way to design metal free carbon electrocatalysts for future green energy applications.

# List of publications

Journal paper:

1. Yaojie Lei[a], Li Wei, Shengli Zhai, Yanqing Wang, H. Enis Karahan, Xuncai Chen, Zheng Zhou, Chaojun Wang, Sui Xiao, and Yuan Chen, Zeolitic Imidazolate Framework Derived Metalfree Bifunctional Carbon Electrocatalysts for Efficient Water Splitting. *Material Chemistry Frontier*, 2018, accepted, DOI:10.1039/C7QM00452D

**Acknowledgments**

First, I would like to express my great gratitude to Professor Yuan Chen, my research supervisor, for always being approachable and providing invaluable advices on many matters, chemical and non-chemical. I would like to thank my co-supervisor, Dr Li Wei, for his continued help during my study. I also want to acknowledge my group members, Shengli Zhai, Xuncai Chen, Zheng Zhou, Adil, Xiao Sui and Chaojun Wang, for their patience and helpful hands. Moreover, the guidance from Dr Jeffery Shi and Dr Tino Kausmann on safety matters are also appreciated. Last but not least, I dedicate this Thesis to my family, and all my friends, for their continued support and extraordinary patience throughout my study.

**Yaojie Lei**

Contents

**Content of Figures.**

List of tables

# 1. Introduction

The increasing public issues about the energy crisis urge the development of sustainable energy as alternatives to replace the fossil fuels. Considering the energy regeneration and environment friendly issues, hydrogen possesses the potential to meet the criterion of renewable and clean energies. Electrochemical water splitting provides a feasible way to produce hydrogen in large-scale. [1-4]

## 1.1 Hydrogen evolution reaction, oxygen evolution reaction and electrocatalyst.

Traditional fuels are replaced with full water splitting by current via electrolyte. During the water splitting, the $H^+$ and $OH^-$ are either "get" or "lose" the electron at the anode and cathode and then generate hydrogen and oxygen, respectively. The reactions are named hydrogen evolution (HER) and oxygen evolution reaction (OER). Kinetic barriers exist in both OER and HER and result in high overpotential requirement. Therefore, efficient electrocatalysts are needed to be used for both the cathodic HER and the anodic OER in a water electrolyser. [3, 4]

## 1.2 Metal-based electrocatalyst.

Precious metals (such as Pt and $IrO_2$) serve as hitherto benchmarking electrocatalysts for either HER or OER, respectively. However, their scarcity and high cost make them impractical for industrial application. [1, 5] In the search for cheap and efficient alternatives, non-precious metal and metal oxides have been used in this direction for replacement of precious metals. All efficient non-noble metal HER electrocatalysts are all based on transition metals, for instance, Co, Ni, Fe, Mo and their derivatives. Nevertheless, due to that unavoidable leaking and corrosion susceptibility, the transition metals are restricted for large-scale commercial production. Therefore, metal-free electrocatalysts should be explored as potential substitutes for metallic electrocatalysts to reduce the cost and enhance the stability of electrocatalysts. [6-9]

### 1.3 Metal free carbon electrocatalysts

Carbon, one of the most abundant elements, can form many allotropes which have unique structural, electrical and thermal properties. Recently, doping heteroatoms (such as C, H, N, O, B, S and P) into carbon structures may result in catalytic activities toward HER and/or OER. [10-24] Such carbon materials are recognized as a new class of cost-effective electrocatalysts for efficient water splitting, which are promising candidates to replace metal based electrocatalysts for practical application in water electrolysers.

#### 1.3.1 Graphene-based electrocatalysts

Graphene and graphene oxide (GO) which are allotrope of carbon are in the form of a 2D, atomic scale. Graphene hexagonal lattices in which one atom forms each vertex, have attracted a lot of attentions because of its physical and chemical properties and eminent electrical conductivity. [25- 27] Nevertheless, owing to no active sites located on the surface of graphene, it always displays poor or no catalytic performance. In recent decades, with functionalization and surface modification of graphene development, the catalytic reactivity of graphene can be improved for applications. On the one hand, by the means of chemical modification, modified graphene (such as, graphene oxide (GO) and reduced graphene oxide) providers for many different oxygenated functional group on the surface of graphene oxide (GO), for instance, -OH, -COOH, $O_x$, and so on. These functional groups are profit for full water splitting. In generally speaking, the structure of graphene and GO mainly are made of $sp^2$ hybridized carbons. After introducing the defects and residual functional groups, $sp^3$ hybridized structure will form and then change electronic properties. These groups on the surface of graphene can easily catch and transfer the electrons from their environment, which make them become efficient candidate for metal-based catalysts. [28, 29] The other promising way to improve the efficiency of water splitting is heteroatom doping. By incorporating N, S, B, P atoms into surface of graphene and GO, the original graphene lattice $sp^2$ structure will be broken and lead to $sp^3$ defects generated, which alters the electronic structure and then improves the electrocatalysts performance. In addition, the DFT

calculations show that N, B, P, S doping on the surface of graphene or GO will decrease the bandgap. Therefore, heteroatoms doping is also an efficient method for increase the both OER and HER performance of graphene and GO. In addition, graphene-based materials are eminent supports for improvement of electrocatalysts performance because of their excellent conductivity and synergistic effect between graphene with other materials. [30-40]

### 1.3.2 Carbon nanotube based electrocatalysts

With allotropes cylindrical nanostructure, carbon nanotubes (CNTs) always exhibit amounts of diversity in their structures, such as diameter, length and chirality. Besides, because of hollow geometry and conjugated π electron structures, carbon nanotubes can show extraordinary thermal conductivity, mechanical and electrical properties. Currently, CNTs have been seen a fast increasing attention in development of CNTs-based materials as efficient catalyst for full water splitting. However, pristine CNTs have very poor electrocatalyst performance towards HER. [41] Thus, some proper methods are needed to change their surface chemistry and electrical structure. Different with heteroatom doping for graphene, DFT results show after doping the nitrogen atom into the CNTs, the electrocatalytic for the HER cannot be improved. [42] In order to improve the electrocatalytic efficiency of CNTs toward the HER, many researches have been explored. Now, there are two methods to change their surface and then increase the HER performance efficiency. First, it is potential to employ combination of other catalytic materials with CNTs. Such promising method can make advantages of both CNTs and other materials "band" together, which make them show not only excellent electrical conductivity of CNTs, but also efficient active sites of other catalytic materials. Through coupling other materials with carbon nanotubes, there will form a strong interaction between them which facilitates the electron transfer and enhances the stability greatly. [43] In addition, surface modification has been proved the feasible way to optimize the HER performance of CNTs. With introducing some acidic groups or oxygenated functional groups, the CNTs will exhibit great improvement for HER performance. For example, after cathodic treatment or acidic oxidation

treatment, many oxygenated functional groups or acidic groups will be formed respectively, which serve as proton relays. All of them acting as proton relays make contribution to the HER. [56]

Recently, with the development of CNTs, some CNT-like materials encounter unprecedented opportunities to expand, for instances, boron nitride nanotubes and carbon nitrogen nanotubes. Many of the new CNT-like materials applied successfully for OER or HER due to more active sites expose on the surface of them.

### 1.3.3 g-$C_3N_4$ and hybrids

With both graphitic and pyridinic nitrogen moieties of g-$C_3N_4$ serving as active sites, graphitic carbon nitride (g-$C_3N_4$) which consists of two earth-abundant elements, carbon and nitrogen, has been explored as electrocatalyst for full water splitting. [44] However, as a semiconductor, g-$C_3N_4$ is subjected to poor electrical conductivity. In order to improve conductivity of g-$C_3N_4$, many strategies have been used to tune its conductivity, such as, hybridizing with conductive carbon substrates (graphene, GO, carbon nanotube, etc.) and heteroatom doping. [45]

### 1.3.4 Other metal-free carbon electrocatalysts for water splitting

Recently polymers have been used as precursor to prepare electrocatalysts for water splitting. For the most of them are composed of earth-abundant elements (C, O, N, S, P, etc.), it can be easily obtained the N, S, P doped carbon-based materials after carbonization at ambient temperature under Ar flow. [46-48] Besides, many organic materials which contain N, P, S etc. have been developed for heteroatom-doped carbon nanomaterials, such as, bacterium, milk powder, hair on human body, etc. The resulted carbon nanomaterials are highly porous which can benefit mass transportation. Meanwhile, these precursors are usually cheap and easily accessible. [49-52]

## 1.4 Importance of Heteroatom doping.

The graphitic structure perfectness, heteroatom doping level and configuration and surface morphology, are important surface chemistry of carbon electrocatalysts which lead to varied catalytic

performance. The graphitic structure perfectness directly relates to the electric conductivity of the resulting carbon materials and contradicts to the defects resulted from heteroatom doping. Theoretical and experimental results suggested by introducing heteroatom dopants, such as boron (B), nitrogen (N), oxygen (O), phosphorus (P) or sulphur (S) into carbon frameworks, the inert carbon surface can be activated to show promising electrocatalytic performance towards various electrochemical reactions, including HER and OER. [10-24] Besides the single element doping, the co-doped engineering of carbon-based material is also an efficient method to change their electronic structure and improve their electrochemical properties. Benefiting from so-called synergistic effect between two various element atoms, co-doped graphitic carbon-based materials show enhanced catalytic activity for OER and HER. In addition, by density functional theory (DFT) calculation, co-doped engineering could change the molecular structure and shift down the valence bands of active sites of carbons, which could boost their HER and OER performance. [13, 18, 55, 56] Mechanism study over the origin of the electrochemical activity indicates that the type and density of the functionalities formed by introducing these heteroatoms are responsible for the observed activity. For example, pydridinic N or ketonic O have been identified as active site for OER [15, 18, 55, 56] while carboxylic groups can serve as proton relays to enhance HER performance [57, 58]. Additionally, the carbon electrocatalysts should also have large surface area and unique porous structures to accommodate more active sites and facilitate good mass transportation during reaction. Therefore, with the aim to design efficient metal-free carbon electrocatalysts for bifunctional HER and OER applications, it is highly desirable to find an effective method to modulate their surface chemistry through tuning the type and density of heteroatom functionalities on carbon surface, which can also help researchers to gain further understanding over the correlation between HER/OER activities and the heteroatom dopants.

However, heteroatoms doping always undergo a harsh reaction environment. Taking annealing for example, thermal annealing performed at high temperature (600~1200 $^{o}$C) is the common method used to dope heteroatoms into carbon framework. [9, 59] The annealing temperature and/or carbon substrate

to dopant molecule ratio are usually controlled with the aim to tune heteroatom loading and configuration in the resulting carbon materials. [10, 16, 18, 60, 61] Therefore, it is essential to develop the new methods to functionalize their surface structures.

**1.5 Cathodic treatment.**

The complicated reaction condition at high temperature always leads to poor control over the type and density of heteroatom containing functional group. Cathodic treatment offers an alternative and promising approach to control the surface functionalities. It can be performed in an aqueous electrolyte at room temperature while the operation parameters, such as treatment time, potential and electrolyte types, can be easily tuned to realize gradual surface chemical property control. Cathodic treatment is post-treatment that by means of the prepared materials being charged with negative potential, the surface of the carbon materials will react with hydrogen ions in an acidic solution and generates oxygenated functional groups, which benefit the HER performance.

Previously, cathodic treatment has been applied on carbon nanotube and bacteria derived carbon materials and improved HER performance has been observed. After the treatment, morphological characterization indicates the alternation in the microstructure of the electrocatalysts. Raman spectroscopy indicates the creation of more defective sites on the carbon structure while detailed Xray photoelectron spectroscopic (XPS) analysis of carbon suggests the formation of more oxygenated functional groups, such as–C=O, -C-O and –COOR, which contribute to the improved HER performance observed on the activated carbon electrocatalysts. Moreover, XPS analysis of heteroatom dopants, such as N and P also indicates the increased population of various N-O and P-O features. Such oxygenated functional groups can serve as proton collectors in favour of adsorbing hydrogen ions through electrostatic interactions. Additionally, they could also serve as proton relays to accelerate the HER kinetic, which shares similar mechanism to that of metal cantered hydrogenase and $C_{60}(OH)_8$. [55, 56]

### 1.6 Metal organic framework based electrocatalyst.

In recent years, metal-organic frameworks (MOFs), which consist of different organic ligands and metal ions though coordination bonds, have attracted tremendous attentions and have been used in many fields. As for the MOF-based carbon materials electrocatalysts, it can be defined as a materials can reserve and transit the energy and reveal preeminent electrochemical activity.[58] Based on previous study, there are two advantages for MOF to be used as carbon-based electrocatalysts.[57] Firstly, through thermal carbonization of MOFs in the inert atmosphere, the graphited structure electrocatalysts with outstanding conductivity can be achieved. Secondly, after carbonization, MOF-based carbon electrocatalysts possess high surface area and uniform pore size distribution. Therefore, MOFs and MOFs-derived porous carbons are always used as both the precursors and templates. However, the performance of MOF-based electrocatalysts may be still inferior to that of Pt-based electrocatalysts. Recent studies indicate cathodic treatment is efficient approach to improve the performance of HER. Thus, that using cathodic activation to improve the catalytic performances of MOE-derived carbon catalysts may be a feasible method.

According to recent study, HER electrocatalysts performance can be affected by the materials containing certain transition metals (such as, Cu, Co, Fe, etc.), but only Zn has been proved to make no difference in HER.16 In order to study the influence of cathodic treatment for MOF-based electrocatalysts, ZIF-8 is the most suitable precursor because of enriched nitrogen content. Nitrogen atoms are incorporated into the aromatic ring, promoting the nitrogen-doped active sites located onto the carbon template. After pyrolysis of ZIF-8, in situ nitrogen-doped carbon-based electrocatalyst will contain a high surface area and their active sites distribute uniformly. [76]

### 1.7 Inspiration and My Research

As aforementioned, herein, by controlling the time of cathodic treatment, I can develop a novel strategy to obtain a series nanoporous carbon electrocatalysts with stepwise modulated surface chemistry, which can lead to tunable HER and OER performance. The carbon material will be obtained

from carbonization of a microporous material, zeolitic imidazolate framework-8 (ZiF-8). ZiF-8 has abundant micro- and mesopores and large surface area (up to 1017 $m^2/g$) which is beneficial for electrochemical reactions.

By adopting various characterization techniques, I can correlate the type and density of surface heteroatom containing functional groups to the treatment time applied, and further with the varied HER and OER performance observed on these carbon electrocatalysts. The optimal treatment time towards obtaining best electrocatalysts for HER and OER can be identified and the performance of the optimal carbon electrocatalysts will be compared with noble metal electrocatalysts (e.g., Pt/C and $IrO_2$/C), which allow them to reach nearly 100 % efficiency in a water electrolyser. My strategy developed here can provide new insight to the surface chemistry of nanoporous carbon material under cathodic treatment with precise control over heteroatom functionalities. It could pave new avenues for the development of metal-free carbon electrocatalysts towards efficient green energy conversion applications.

# 2. Experimental Section

## 2.1 Material synthesis.

In my study, zeolitic imidazolate framework-8 nanopowder was purchased from Sigma-Aldrich and used as received. Porous carbon material was obtained by carbonization of ZIF-8 powder at 900 ºC for 3 hours under 100 sccm argon (99.99%, Coregas) flow. This condition was chosen based on previous study where ZiF-8 was used to prepare carbon materials for supercapacitor applications. The material obtained under the chosen condition showed the best surface area and electric conductivity, where are important for electrocatalysis. [76] The resulted carbon materials were washed with 1 M HCl solution overnight to remove residual Zn, collected by vacuum filtration and subsequently resined with DI water. The powder was dried in vacuum overnight and denoted as C0 sample.

## 2.2 Surface chemistry modulation by cathodic activation.

The as prepared C0 sample was dispersed in iso-propanol (IPA) by bath sonication and loaded on a piece of carbon cloth (2 × 2 $cm^2$) at an aerial mass loading of 2.5 $mg/cm^2$. The cathodic modulation was performed under a three-electrode configuration in a two-chamber electrochemical cell separated by glass frit. 0.5 M $H_2SO_4$ was used as electrolyte. The carbon cloth loaded with C0 was used as working electrode in one chamber. In another chamber, a graphite rod was used as counter and a saturated calomel electrode (SCE) was used as reference electrode. Afterwards, the working electrode was cathodic treated at –2 V *vs.* SCE for 2, 4, 6 and 8 hours by continuous discharging and the materials obtained from different treatment time was denoted as C2, C4, C6 and C8, respectively. (Different electrolytes, concentration electrolytes, potential as well as treatment time have various effects for the result of cathodic polarization treatment) After treatment, the carbon material was recovered by bath sonication of the carbon cloth electrode in 10 mL IPA. The weight of C2~C8 samples were determined by weighting the solid materials obtained after drying using an analytical balance.

### 2.3 Physiochemical property characterization.

The properties of the C0~C8 samples were characterized by a comprehensive set of techniques. The surface morphology was examined by a field-emission scanning electron microscope (FE-SEM, Jeol, JSM-6700F). Elemental distribution was tested by energy-dispersive X-ray spectroscopy (EDX) mapping on the same FE-SEM. Specific surface areas were measured using a surface area analyser (QuantaChrome, Autosorb-6B) and calculated by the Brunauer–Emmett–Teller (BET) method. Pore diameter distribution was calculated from the $N_2$ physisorption isotherms using the non-local density functional theory (NL-DFT) method. Raman spectra were recorded on a Raman microscope (Renishaw inVia) in the backscattering configuration under a 514 nm (2.41 eV) laser. The chemical composition of the material surfaces and heteroatoms was analysed by X-ray photoelectron spectroscopy (XPS, PHI5000 Versa Probe III) equipped with an Al-Kα (1486.3 eV) radiation source.

### 2.4 Electrode preparation.

For all electrochemical test, a single glassy carbon (GC) electrode was used (3mm diameter, 0.07 $cm^2$, CHI Instrument). C0~C8 samples were dispersed in a 1/9 (v/v) water-iso-propanol solution containing 0.05 wt% Nafion at a concentration of 1 mg/mL by bath sonication. About 20 μL electrocatalyst ink was then dropped casted on the GC electrode, resulting an aerial mass loading of ~0.3 $mg/cm^2$. For each experiments, three electrodes were prepared and tested. Commercial 20 wt% Pt/C and $IrO_2$/C catalysts (Sigma) was loaded on the GC electrode at the same loading for comparison.

### 2.5 Electrochemical performance test.

All electrochemical test was performed on a CHI660E electrochemical workstation (CHI Instrument) under three electrode configuration in a two-chamber electrochemical cell unless stated otherwise. A graphite paper (2.5 × 2.5 $cm^2$) and a SCE was used as counted and reference electrode. Hydrogen evolution (HER) performance was assessed in 0.5 M $H_2SO_4$, 0.5 M potassium phosphate buffer (PBS, pH=7) and 0.1 M KOH electrolytes saturated with $H_2$. Oxygen evolution (OER) tests were carried out in 0.5 M PBS (pH=7) and 0.1 M KOH saturated with $O_2$. Linear sweep voltammetry (LSV) curves

were obtained at a scan rate of 5 mV/s with 95% *iR*-compensation. Tafel plots were collected at a scan rate of 0.2 mV/s.

# 3. Results and Discussion

## 3.1 Preparation of surface modulated carbon electrocatalysts

The production of carbon electrocatalysts starting from ZIF-8 is illustrated in Scheme 1. First, the ZIF-8 MOF particles are pyrolyzed at 900 ºC to produce the N-doped and heteroporous carbon material (ZIF-8-C0). During pyrolysis, the imidazole rings expectedly serve as the main source of graphite-like carbon framework formation, and high N content of ZIF-8 (*i.e.*, two N atoms per ligand, 2methylimidazole) serves as chemical dopants. Then, by the removal Zn residues with acid leaching using dilute HCl, and water rinsing, I achieved the chemically doped and heteroporous carbon framework. Next, applying cathodic polarization treatment at –2.0 V *vs.* SCE on ZIF-8-C0 loaded on carbon cloth over different periods of time (2–8 hours), I have modulated the type and relative abundance of different surface functional groups, resulting in a series of carbon materials (ZIF-8C2~C8). To avoid the contamination from any Pt dissolution [65, 66], the cathodic polarization was carried out in the two-cell electrolyzer separated with a 4-mm glass frit, and the carbon electrode (graphite rod) was used as the counter electrode.

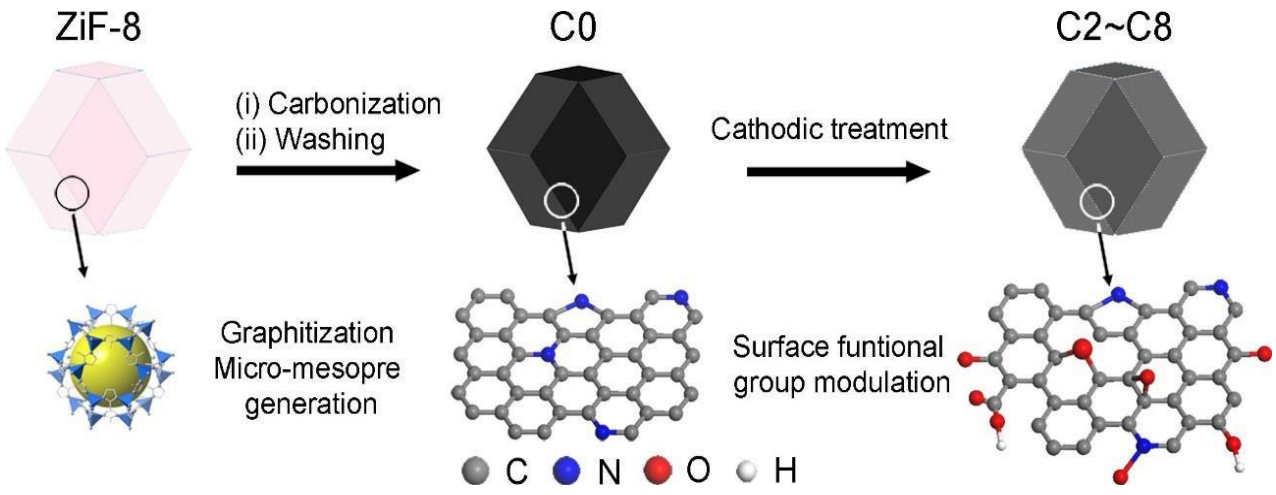


**Scheme 1.** Scheme of the preparation of surface modulated carbon electrocatalysts.

### 3.2 Physiochemical property characterisation

#### 3.2.1 Surface morphology of various carbon electrocatalysts

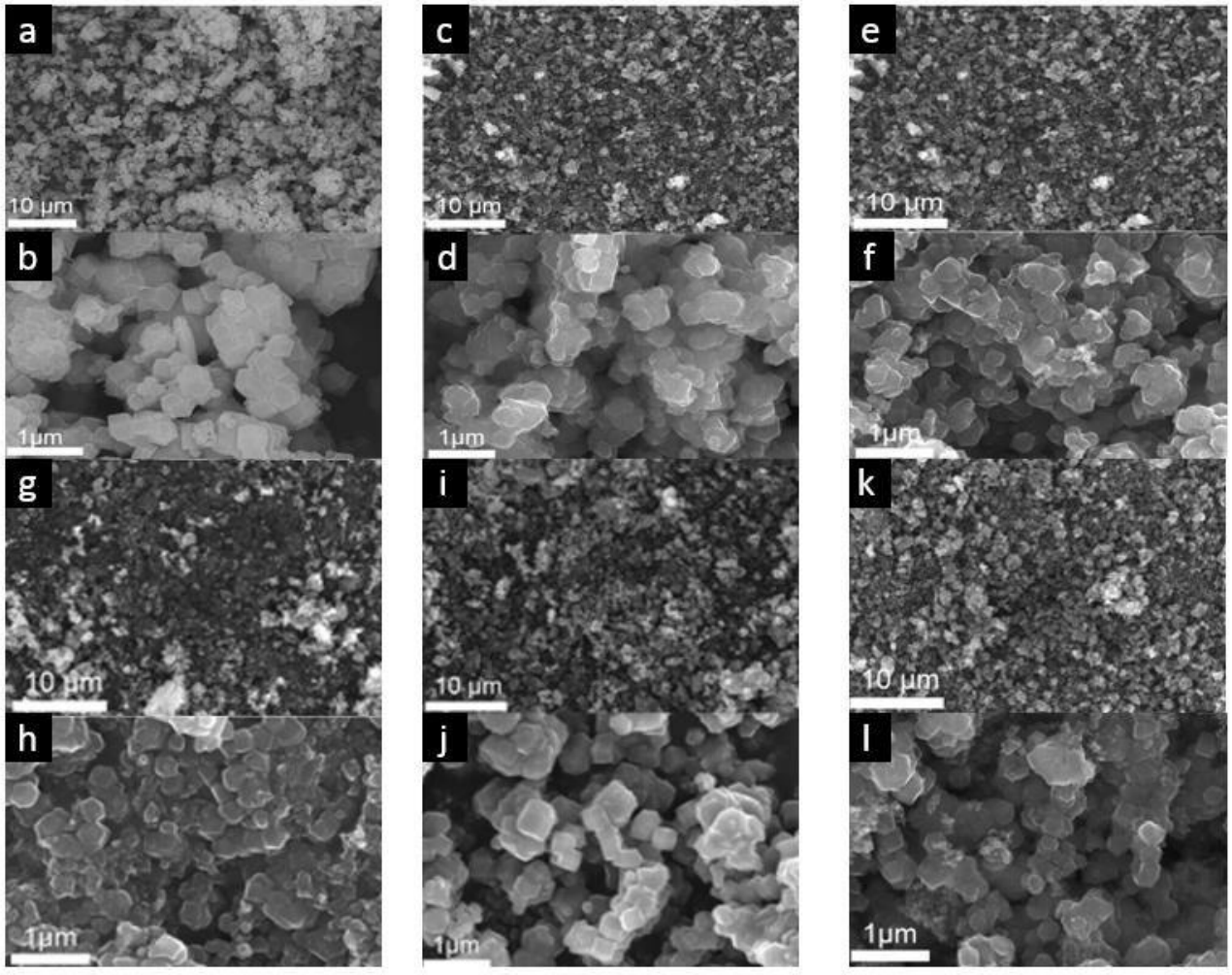


**Figure 1**. SEM images of (a) and (b) ZiF-8 particles, (c) and (d) C0, (e) and (f) C2, (g) and (h) C4, (i) and (j) C6, (k) and (l) C8 samples at different magnification.

The physicochemical properties of the carbon materials were examined by several characterization techniques. Using SEM, I have compared the morphological properties of untreated, pyrolyzed, and cathodic polarization treatment applied ZIF-8 particles (see Figure. 1). ZIF-8 particles retained their polyhedron shape upon pyrolysis at 900 °C (compare untreated ZIF-8 particles seen in Figure. 1a–b with ZIF-8-C0 particles in Figure. 1c–d). And importantly, the morphology of ZIF-8-C2 (Figure. 1e-

f), ZIF-8-C4 (Figure. 1g-h), ZIF-8-C6 (Figure. 1i–j) and ZIF-8-C8 (Figure. 1k-l) showed minor deviations from the shape of ZIF-8-C0 after being exposed to cathodic polarization treatment, suggesting that our post-carbonization treatment routine made a minor impact on the overall structure of the ZIF-8-derived carbon materials.

As explained above, the overall shape characteristics of ZIF-8 particles can be preserved even after the longest cathodic polarization treatment. Therefore, given ZIF-8 is an intrinsically super porous material, pyrolysis treatment inevitably creates volatile materials, and leaching out of residuals Zn should leave voids behind; one may expect the formation of different levels of porosities. Nevertheless, to obtain a more precise idea regarding the specific surface area and pore distribution of the carbon materials, I performed $N_2$ physisorption analysis. Physisorption isotherms in Figure. 2a show mixed Type I and IV isotherms [67]. The sharp uptakes at the low-pressure region ($P/P_0 < 0.15$) indicate the existence of micropores, while the hysteresis at the medium pressure region ($0.45 < P/P_0 < 0.8$) suggests the presence of mesopores. And importantly, pore size distributions calculated by the NLDFT method show similar porosities for all samples, with micropores centered on 1.1 nm and mesopores at around 4.8 nm (Figure. 2b), which is in agreement with earlier reports on the carbonization of ZIF-8 for other purposes [68, 69]. With the extension of the cathodic polarization treatment duration from 2 to 4, and 6 to 8 hours, the pore size distributions became slightly wider, which may be attributed to the minute physical changes in porosities as well as the variation of functional group composition. A previous study reported that surface functionalities can alter the pore edge structures of porous carbon materials, resulting in a wider pore size distribution [70]. Consequently, as shown in Table 1, 2 hours of cathodic polarization treatment caused only around 4.5% drop in the specific surface area (from 1017 to 961 $m^2/g$). And, the extension of the treatment time from 2 to 8 hours showed a steadily declining trend from 961 to 908 $m^2/g$ with ~2% drop per 2 hours. Nevertheless, ZIF-8-C8 still retains a large specific surface area, *i.e.*, ~90% of the as-pyrolyzed material.

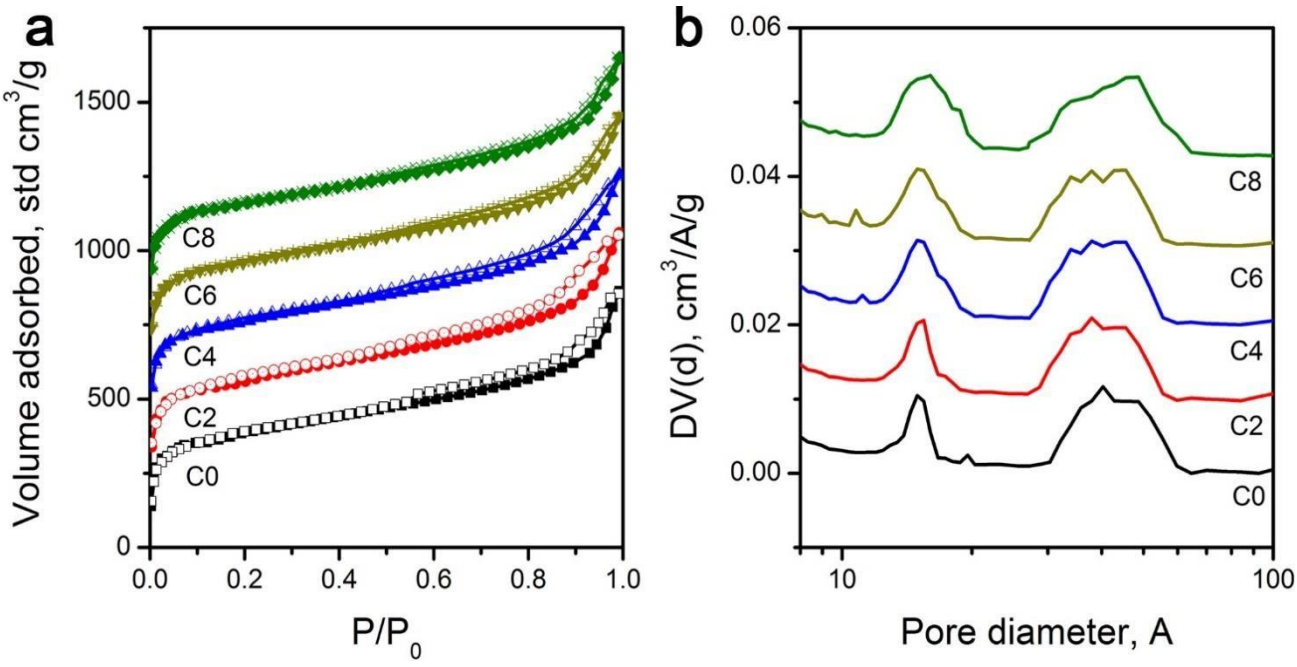


**Figure 2**. (a) N2 physisorption isotherms and (b) pore size distribution of various samples. (c) Specific surface area and calculated Raman ID/IG ratio of various samples

**Table 1**. Physicochemical properties of ZIF-8-derived carbon materials upon the cathodic treatment at different durations.

| ZIF-8- | SSA, $m^2/g$ | ID/IG | *La* nm | Elemental abundance at. % | | | ECSA |
|---|---|---|---|---|---|---|---|
| | | | | C | N | O | Normalized $m^2/g$ |
| 0 | 1017 | 1.04 | 4.20 | 90.8/90.7 | 8.4/8.3 | 0.8/1.0 | 785.7 |
| 2 | 961 | 1.09 | 3.98 | 90.5/90.3 | 7.5/7.3 | 2.0/2.4 | 764.3 |
| 4 | 947 | 1.16 | 3.75 | 86.4/85.9 | 6.5/6.4 | 5.1/7.3 | 740.5 |
| 6 | 923 | 1.25 | 3.48 | 83.5/82.7 | 5.4/5.1 | 11.1/12.2 | 706.0 |
| 8 | 908 | 1.31 | 3.32 | 79.5/78.9 | 1.9/1.3 | 18.6/19.8 | 557.7 |

Raman spectra of the carbon materials are shown in Figure. 3. The strong graphitic band (G-band) located at ~1600 $cm^{-1}$ can be found in all carbon materials, suggesting the formation of graphitic structures upon pyrolysis. The defect induced D-band peaks (at ~1300 $cm^{-1}$) got larger from of ZIF8-C0 to C8. The intensity ratio between the D-band and the G-band ($I_D/I_G$) is tabulated in Table 1, showing the continually increasing trend, which may be due to defect formation and chemical doping. The in-plane coherence length ($L_a$) provides the mean average crystallite size of $sp^2$-hybridized carbon domains in the graphitic carbon framework [68]. $L_a$ can be calculated from the $I_D/I_G$ ratio using $L_a$=C(λ)/($I_D/I_G$) with C(λ) of 4.35 nm for the 514 nm laser used, and the results are summarized in Table 1. The $L_a$ value decreases from 4.20 nm of ZIF-8-C0 to 3.32 nm of ZIF-8-C8, indicating that the cathodic polarization treatment changes the surface properties of the carbon materials.

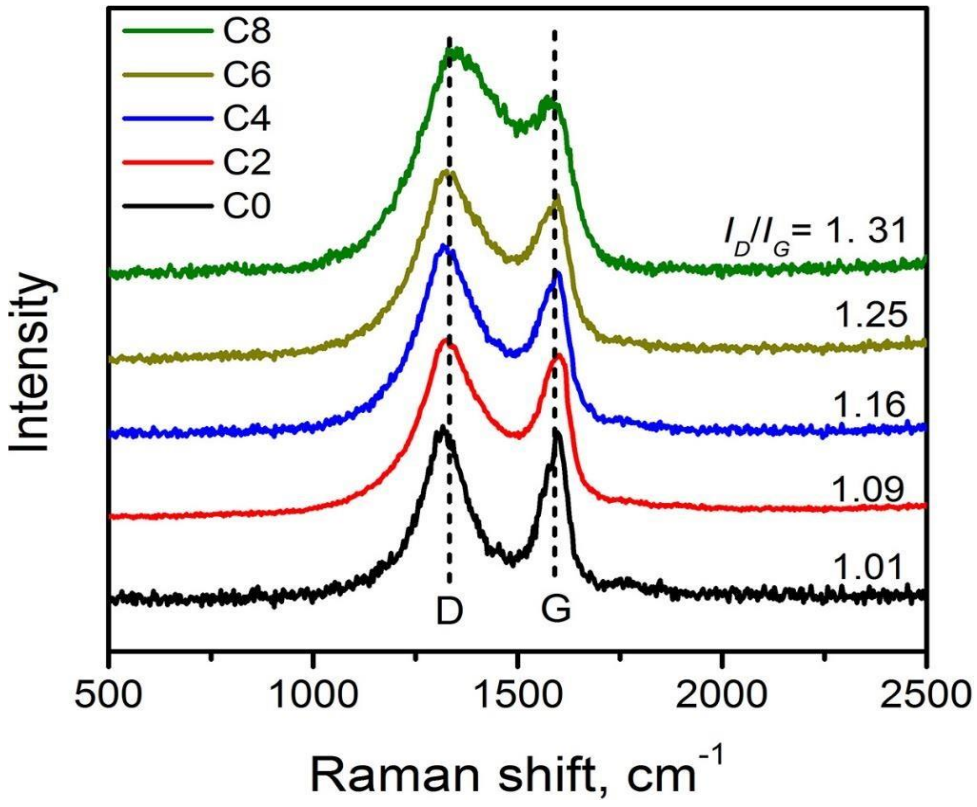


**Figure 3**. Raman spectra of carbon electrocatalysts.

The electrochemical active surface area (ECSA) of various ZIF-8-derived carbon electrocatalysts were determined by measuring their electrochemical double layer capacitance using the carbon cloth

electrodes in 0.5 $H_2SO_4$ electrolyte, and the results are shown in Table 1 and Figure. 4. The cathodic activation induced minor decreases in the ECSA of the ZIF-8-derived carbon electrocatalysts.

Comparing with the 785.7 $m^2/g$ of ZIF-8-C0, the ZIF-8-C4 and ZIF-8-C6 retained the large ECSA of 740.5 and 706.0 m2/g, respectively. Prolonged cathodic polarization will introduce more defect sites on the carbon basal plan, which will result in reduced ECSA.

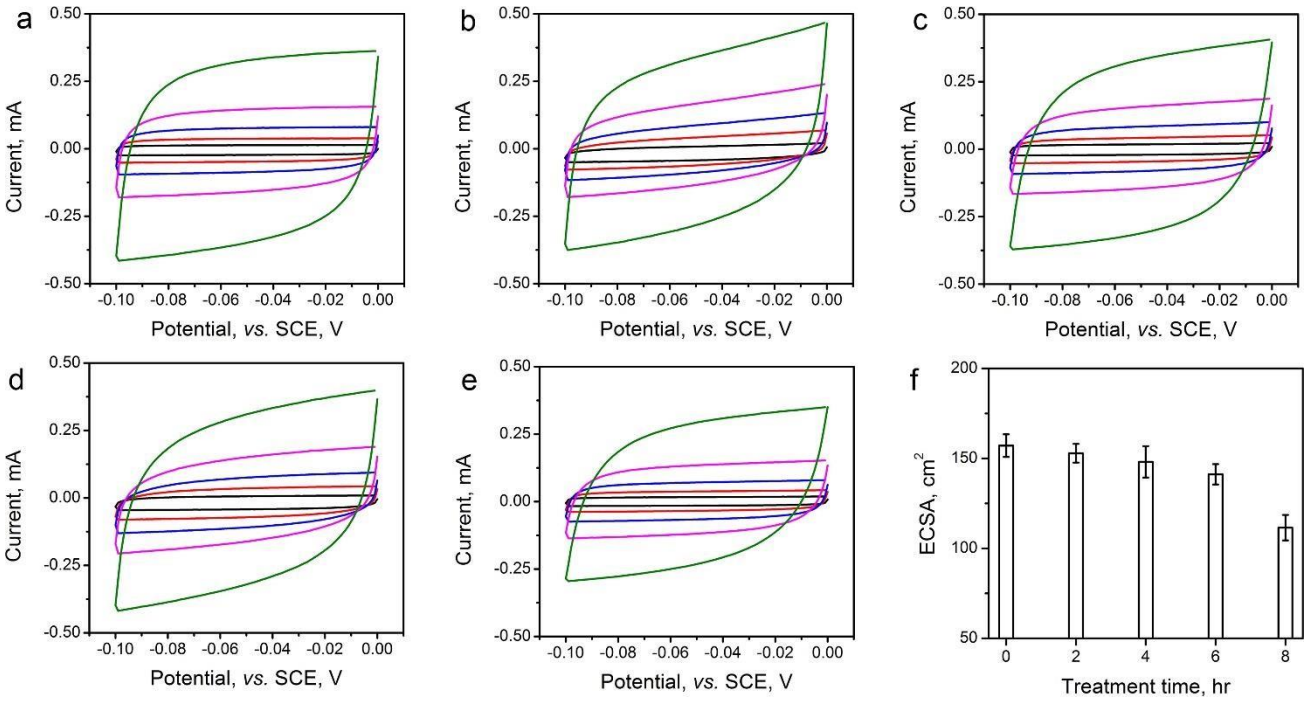


**Figure 4**. Cyclic voltammetry (CV) scan curves of various carbon electrocatalysts obtained at scan rates of 5 to 50 mV/s.

### 3.2.2 EDX elemental mapping and C, N, O abundance of different samples.

From the Figure 5a, the elemental composition of the C0-C8 samples are measured by energy dispersive X-ray spectroscopy (EDX) mapping scan. From the images, three elements (C, N, O) exist in samples. Inductively coupled plasma atomic emission spectroscopy (ICP-AES) is further applied to detect metal elements, with no Zn residual or Pt contaminants found. As shown in Figure 5b, the elemental composition of carbon electrocatalysts is changed when they are modulated by the different treatment time. C0 sample possesses the highest nitrogen content (8.4 at%) and the lowest oxygen

content (0.8 at%). With the cathodic treatment time increasing, the oxygen content successively increases, suggesting cathodic treatment creates more oxygenated functional groups. At the same time, some nitrogen functional group will be removed, resulting in a decreasing tendency of N content. [72] Consequently, the C8 sample has the lowest N content 1.9% and the highest O content 18.6%. Element analysis suggests cathodic treatment is the efficient method to create functional groups on the surface of carbon materials.

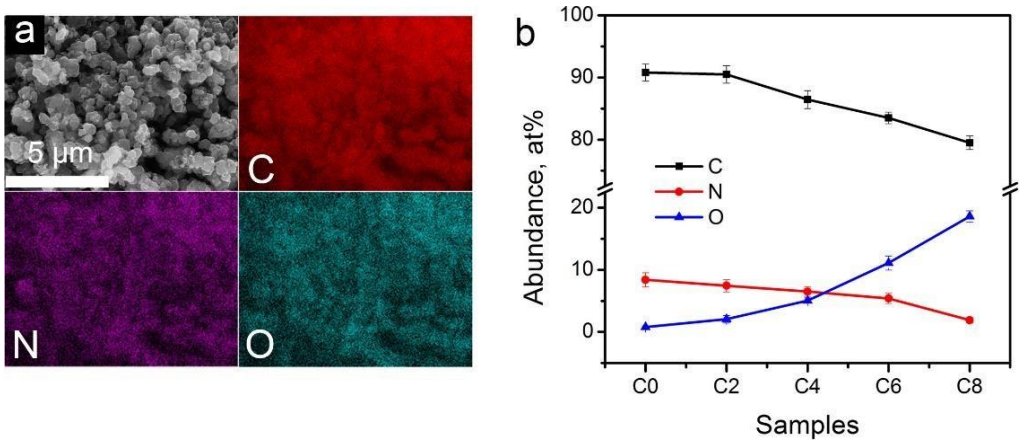


**Figure 5**. (a) SEM image and EDX elemental mapping result of C6 sample and (b) C, N and O abundance in C0~C8 samples.

### 3.2.3 XPS analysis of C, N, O elements in different samples

It is necessary to study the strong relationship between type and density of the functional group with HER and OER performance of the MOF derived carbon electrocatalysts. To explore the type and abundance of different functional groups, X-ray photoelectrospectrocopy (XPS) analysis is used to scan the C0-C8 samples. Survey scans of the carbon electrocatalysts are shown in Figure 6 with the peak intensity change of N and O in good agreement with the elemental composition information obtained from EDX mapping.

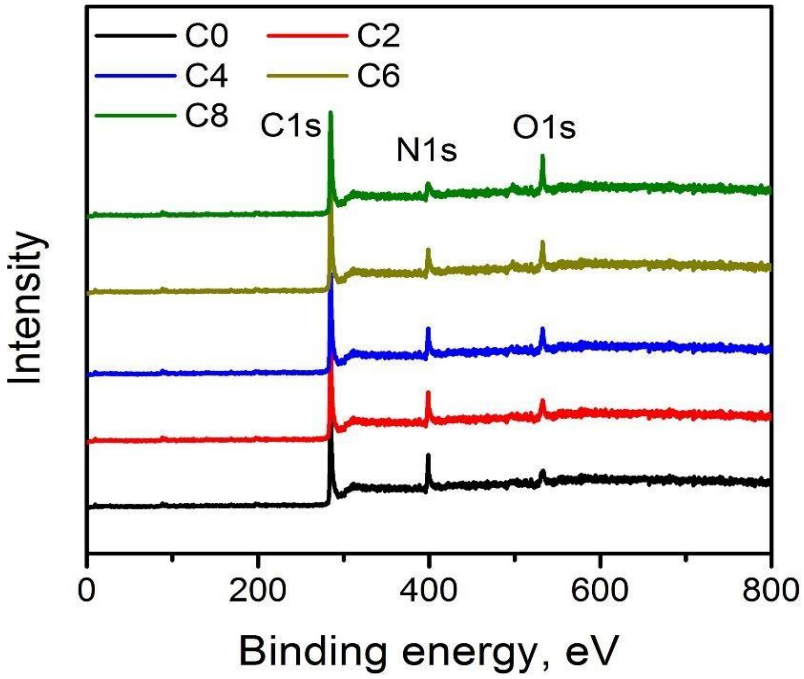


**Figure 6**. XPS survey scan of C0~C8 samples.

Specially, XPS survey scans shown in Figure. 7-9 and the variations in the peak intensity of N and O agree with the elemental composition changes observed in EDX (Table 1). High-resolution XPS scans of C, N, and O in Figure. 7-9 show notable spectral changes, indicating that the cathodic polarization treatment alters the surface functional group compositions significantly. The spectrum deconvolution was performed to determine the detailed changes in the C, N, and O-containing surface functionalities (see Figure. 7-9). The relative abundance of C, N, and O in different functional groups is tabulated in Table A1. Combing the Figure 7 and Table A1, the $sp^2$-hybridized C in the graphitic carbon framework is the major C species in all materials with the relative abundance above 60%. The abundance of C in ketonic and carboxylic groups continually increases with the extension of the treatment duration, and reaches the maximum in ZIF-8-C8, indicating the formation of oxidized C functionalities during the cathodic treatment. N-containing functionalities also show a systematic change. Figure. 8 indicates that oxidized N functionalities are virtually absent in ZIF-8-C0, while their relative abundance increases with the application of cathodic treatment. In contrast, the abundance of pyridinic, pyrrolic, and graphitic N functionalities decreases. Figure. 9 shows that the cathodic treatment also creates more oxygenated functional groups. Only 0.8 at.% O in ZIF-8-C0 can be

assigned to chemisorbed water. After 2 hours of cathodic treatment, nearly 60% of O is in the form of hydroxyl or epoxy functional groups. And after 4 hours of cathodic treatment, these functionalities are oxidized to ketonic or carboxylic functional groups. Further treatment converts part of the ketonic groups into carboxylic groups. Overall, EDX and XPS results show that the cathodic treatment is an efficient method to modulate the type and density of the surface functional groups on the ZIF-8-derived carbon materials.

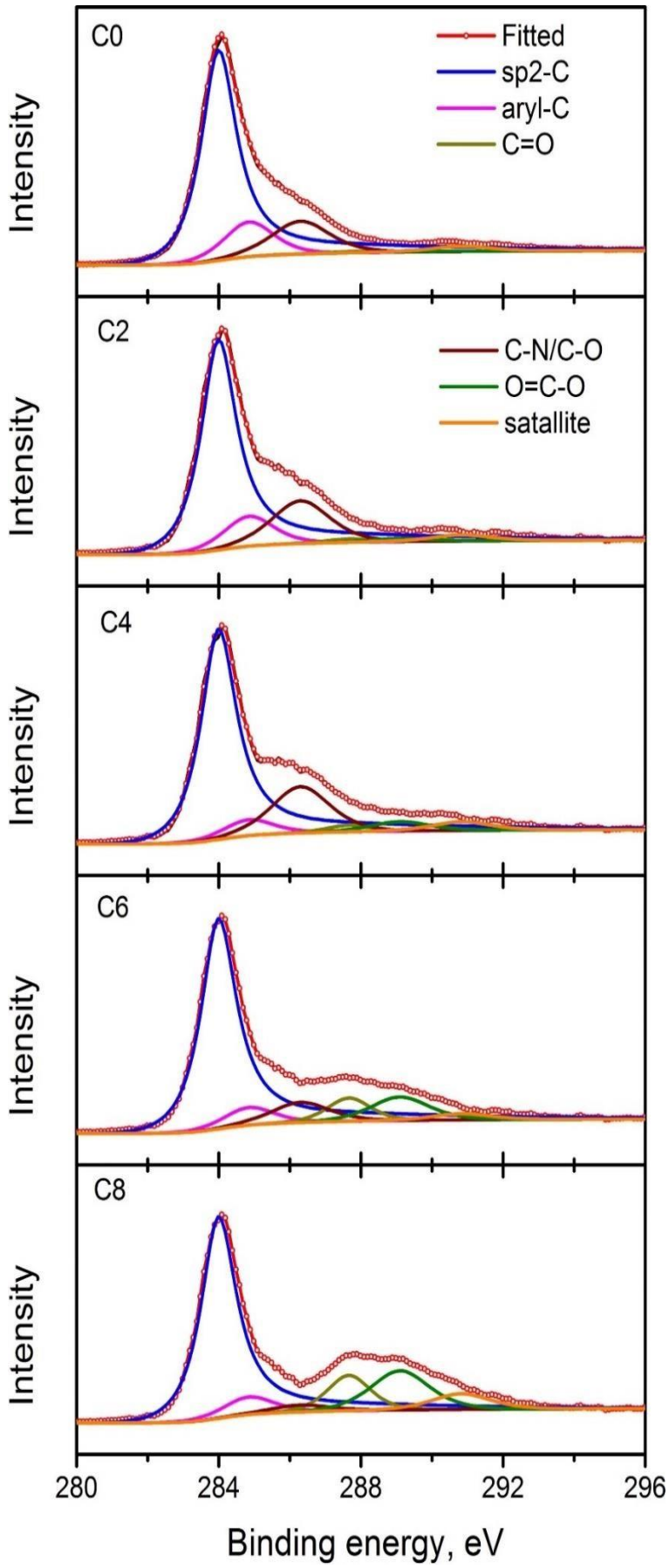


**Figure 7**. High resolution XPS spectra of C in various carbon electrocatalysts.

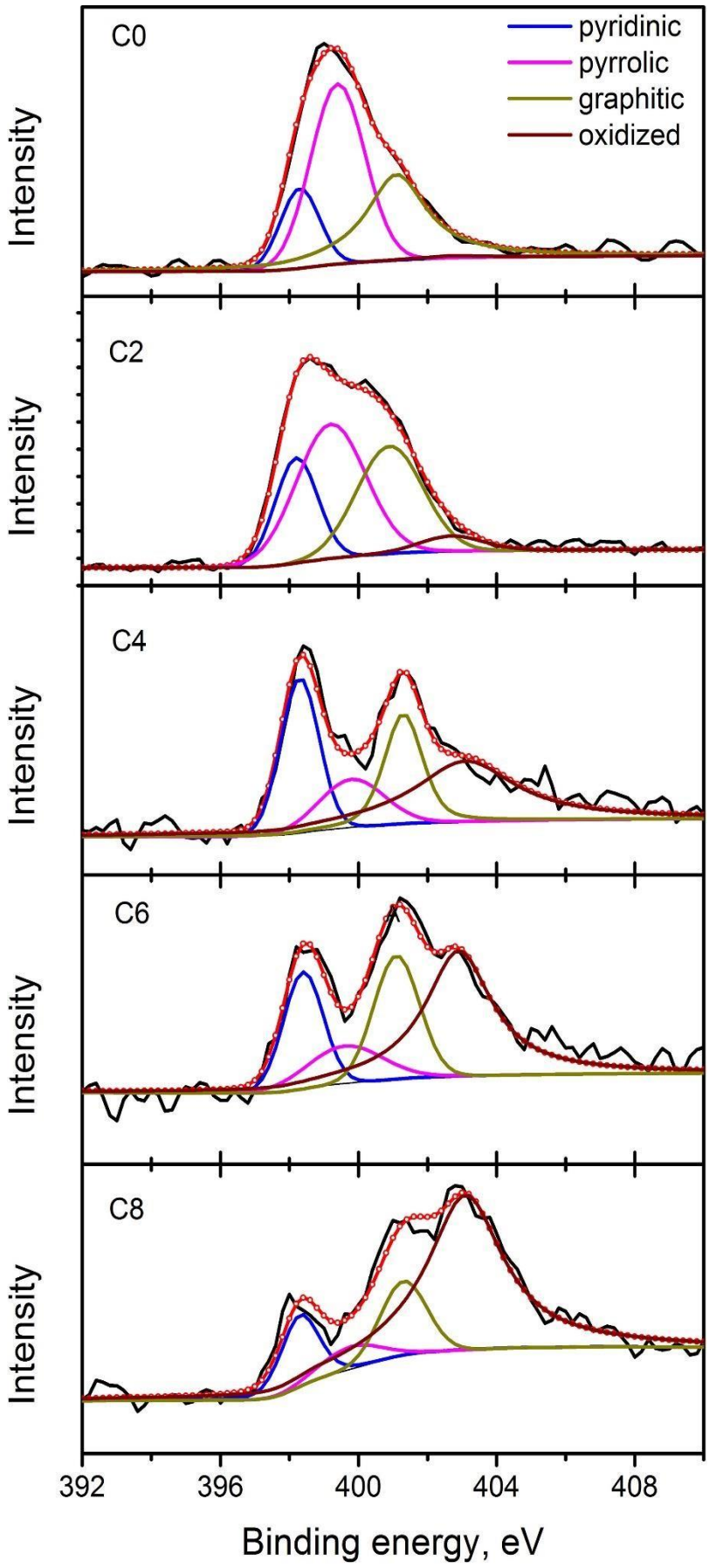


**Figure 8**. High resolution XPS spectra of N in various carbon electrocatalysts

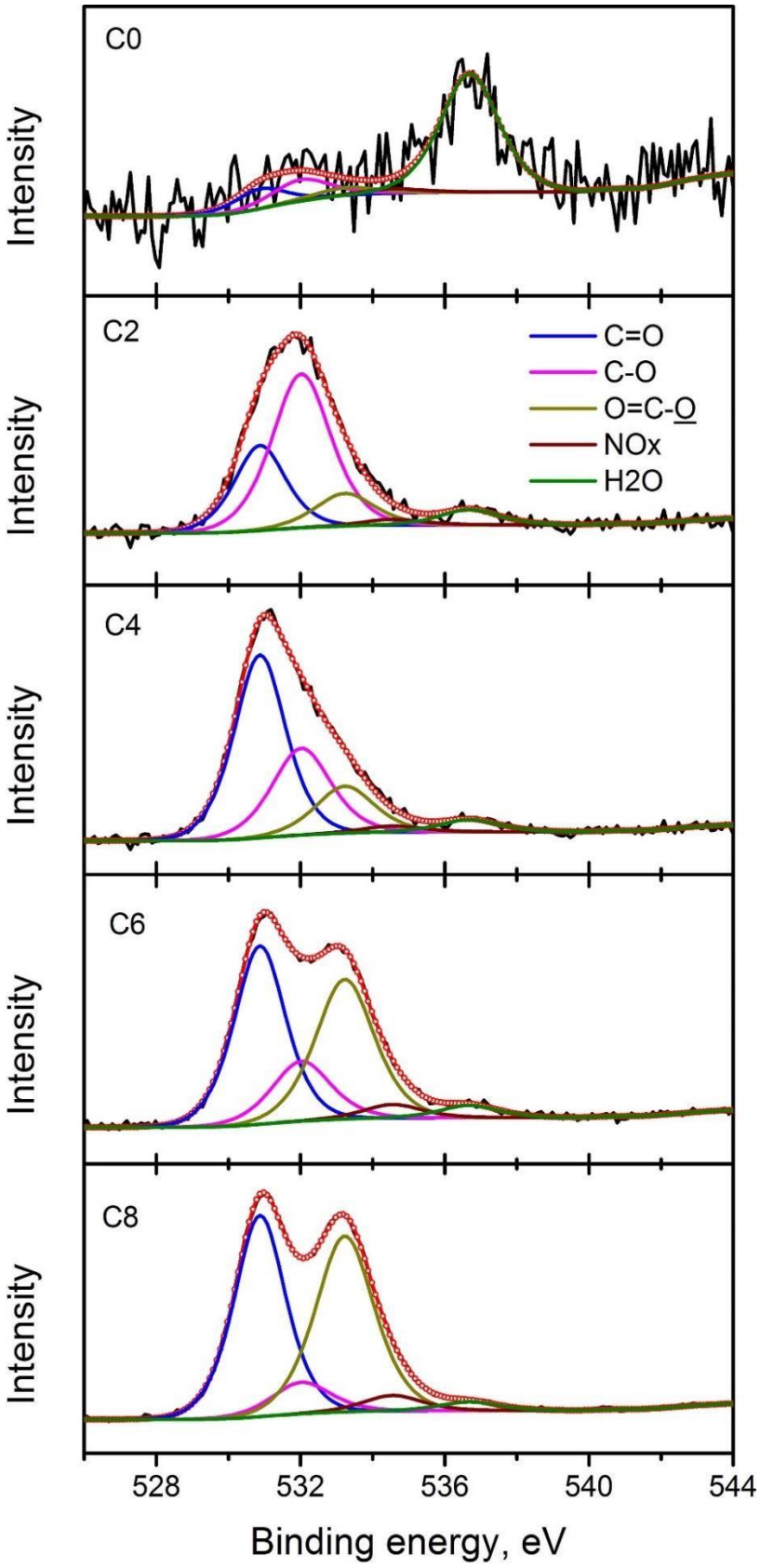


**Figure 9**. High resolution XPS spectra of O in various carbon electrocatalysts.

### 3.3 Hydrogen evolution performance of various samples in different solvents

First, in order to avoid the effect of carbon cloth (carbon cloth can be activated by cathodic treatment), the ZIF-8 was activated on the carbon cloth and then stripped by sonication. The electrocatalytic activity for HER from the ZIF-8-derived carbon electrocatalysts was evaluated in a $H_2$-saturated acidic electrolyte (0.5 M $H_2SO_4$). The LSV curves are shown in Figure. 10a. The analysis results are summarized in Table 2 for comparison based on the three performance parameters: i) overpotential, ii) Tafel slope, and iii) exchange current density. The overpotential required to reach the geometric current density ($j$) of 10 mA/cm$^2$ ($\eta_{10}$) is the first performance parameter considered. The value of $\eta_{10}$ gradually decreases from ~451 mV of ZIF-8-C0 to 155 mV of ZIF-8-C6. However, it increases to 170 mV of ZIF-8-C8, suggesting that extended cathodic treatment is not desirable. The second parameter, the changed Tafel slopes, indicates that the HER reaction kinetics on the various carbon electrocatalysts is different. The Tafel slope of ZIF-8-C0 and ZIF-8-C2 is 179.3 and 146.5 mV/dec, respectively, suggesting that the initial $H^+$ adsorption (the Volmer step) is the rate-limiting step on these two electrocatalysts. The Tafel slope of ZIF-8-C4 decreases to 116.5 mV/dec, indicating that the rate-limiting step shifts to the electrochemical desorption (note that the Heyrovsky step has the Tafel slope at 40~120 mV/dec). The Tafel slope of ZIF-8-C6 is the smallest at 54.7 mV/dec. However, it increases to 68.5 mV/dec for ZIF-8-C8. ZIF-8-C6 shows the best HER kinetic performance among the five ZIF-8-derived carbon electrocatalysts. The Tafel slope of ZIF-8C6 approaches that of the state-of-the-art commercial 20 wt.% Pt/C (34. 7 mV/dec) catalyst. Similarly, the third performance parameter, the exchange current density ($j_0$) calculation was obtained from extrapolation of the Tafel by fitting the linear part of the Tafel plot by following equation:

$$\eta = b \log j + a$$

Where a is intercept on the y-axis and b is the Tafel slope. $j_0$ is determined when $\eta$= 0V.

After calculation, ZIF-8-C6 is the highest at 0.063 mA/cm$^2$, which is more than two times larger than that of the our previously reported N and P dually doped carbon electrocatalysts [55]. Meanwhile,

to further assess C6 electrocatalyst practical use, the performance of C6 sample is compared with recent metal-free electrocatalysts in both 0.5 M $H_2SO_4$ and 0.1 M KOH in Table A3 and Table A4, respectively. Compared with other metal-free electrocatalysts, C6 shows good performance. Therefore, the results for the HER reactions suggest that

C6 could be an active electrocatalyst for overall water splitting.

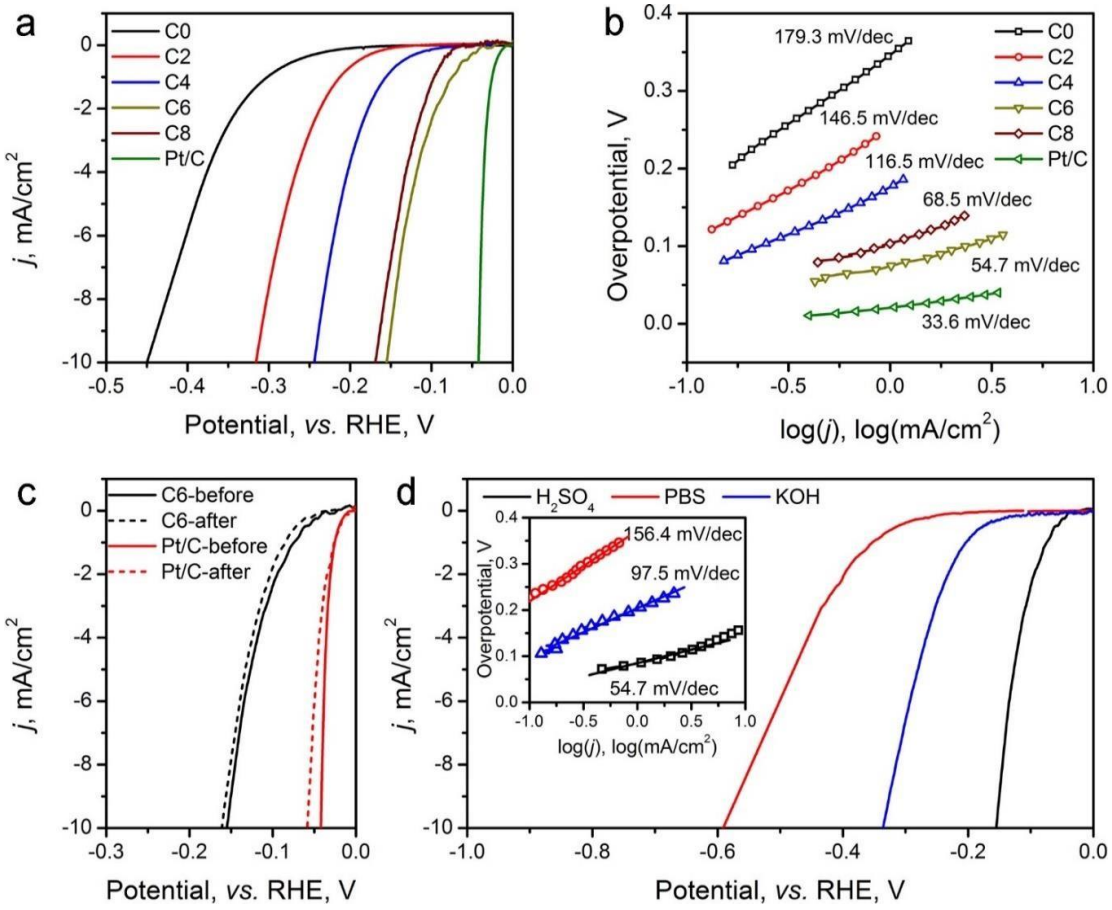


**Figure 10**. HER performance of C0-C8 electrocatalysts in 0.5 M H2SO4 electrolyte. (a) LSV polarization curves and (b) Tafel plots. (c) Stability test of C6 electrocatalysts in comparison with Pt/C before and after 2000 cycle CV scan between 0 to –0.4 V (vs. RHE) in 0.5 M H2SO4. (d) HER performance of C6 catalyst in neutral 0.5M PBS and 0.1M KOH. Inset: Tafel plots.

**Table 2**. HER performance of C0-C8 samples (0.5 M $H_2SO_4$)

| | $\eta_{10}$, mV | Tafel slope, mV/dec | $j_0$, mA/cm$^2$ |
|---|---|---|---|
| C0 | 451 | 179.3 | 0.010 |
| C2 | 316 | 146.5 | 0.016 |
| C4 | 245 | 116.5 | 0.027 |
| C6 | 155 | 54.7 | 0.063 |
| C8 | 169 | 68.5 | 0.049 |

Next, the electrocatalytic durability of the optimal ZIF-8-C6 was compared with that of the commercial Pt/C catalyst. First, the cycling test was conducted in 0.5 M $H_2SO_4$ from –0.2~0 V (*vs.* RHE) at the scan rate of 50 mV/s for 2000 cycles. The LSV curves obtained before and after the cycling test are shown in Figure. 10c. The $\eta_{10}$ value of ZIF-8-C6 increases by merely 8 mV, which is much smaller than the 18 mV increment of Pt/C. Next, the chronoamperometric test was carried out in 0.5 M $H_2SO_4$ at 10 mA/cm$^2$ for 10 hours (see Figure. 11). The overpotential required by ZIF-8-C6 increases by ~4.4%. In comparison, it increases by ~12.5% for the commercial Pt/C catalyst. These two tests indicate the excellent durability of ZIF-8-C6. Last, the HER electrocatalytic activity of ZIF8-C6 in neutral or basic electrolytes was also tested, and the results are shown in Figure. 10d. The $\eta_{10}$ value and Tafel slope increase marginally to 590 mV and 156.4 mV/dec in 0.5 M neutral PBS (pH=7) solution and 336 mV and 97.5 mV/dec in 0.1 M KOH. These results show that it is feasible to apply ZIF-8-C6 for $H_2$ production in water electrolyzers with neutral or basic electrolytes.

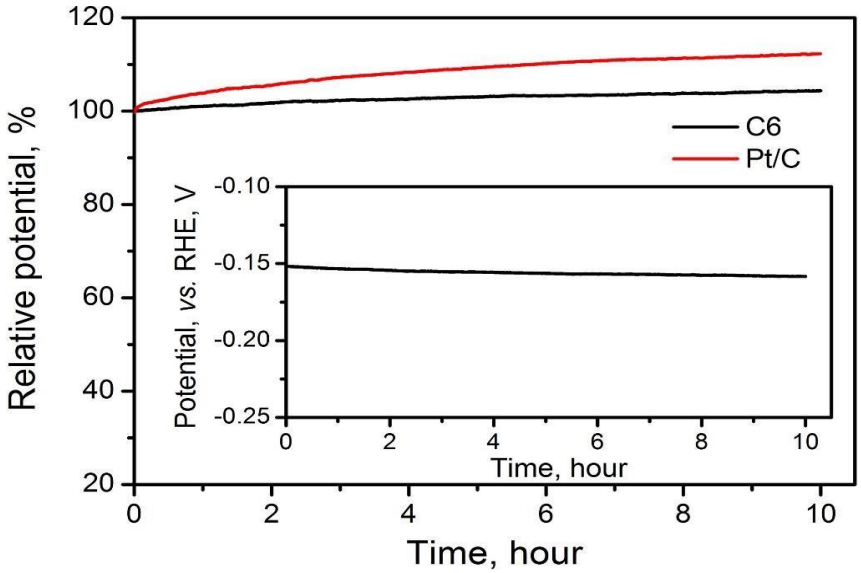


**Figure 11**. HER test of the C6 sample performed at 10 mA/cm2 in 0.5 M H2SO4 electrolyte. Inset: chornoampermetric curve of C6 sample.

### 3.4 Oxygen evolution performance of different samples in different solvents

The OER activity of the ZIF-8-derived carbon electrocatalysts was evaluated in $O_2$-saturated 0.1 M KOH electrolyte, and the results are shown in Figure. 12a-b and Table 3. Similar to their electrocatalytic activity for HER, Figure. 12a shows that their electrocatalytic activity for OER strongly depends on the cathodic polarization treatment. ZIF-8-C0 has the largest $\eta_{10}$ of 798 mV and Tafel slope of 192.1 mV/dec. These values decrease with the extension of the cathodic polarization treatment duration. ZIF-8-C4 has the smallest $\eta_{10}$ at 476 mV and the Tafel slope at 78.5 mV/dec, exhibiting one of the best performances among recently reported carbon OER electrocatalysts, such as surface N-enriched CNTs ($\eta_{10}$ = 510 mV) [20], N,O-dually doped carbon hydrogel (564 mV at 14.8 mA/cm$^2$ and 141 mV/dec) [73], few-layer N-doped graphene ($\eta_{10}$ > 1 V) [74], and $C_3N_4$-graphene hybrid ($\eta_{10}$ = 539 mV) [75]. However, the electrocatalytic activity deteriorates when the cathodic polarization treatment duration goes beyond 4 hours. Furthermore, to obtain a deeper understanding regarding the nature of observed high performances, I have performed electrochemical impedance spectroscopy (EIS) analysis on the ZIF-8-derived carbon electrocatalysts at the overpotential of 0.3 V in 0.1 M KOH electrolyte. The Nyquist plots were fitted with the Randel circuit to estimate the electrocatalysts' polarization

resistance ($R_P$) (see Figure. 13). ZIF-8-C0 has the largest $R_P$ of 70.4 ohm. $R_P$ quickly decreases to the minimum of 17.78 ohm for ZIF-8-C4, but it increases with the extension of cathodic polarization treatment duration. The lowest polarization resistance of ZIF-8-C4 is also a contributing factor to the observed high electrocatalytic activity.

**Table 3**. The OER performance of C0-C8 samples

| Sample | $\eta_{10}$, mV | Tafel slope, mV/dec |
|---|---|---|
| C0 | 798 | 192.1 |
| C2 | 620 | 167.2 |
| C4 | 476 | 78.5 |
| C6 | 528 | 91.9 |
| C8 | 570 | 139.4 |

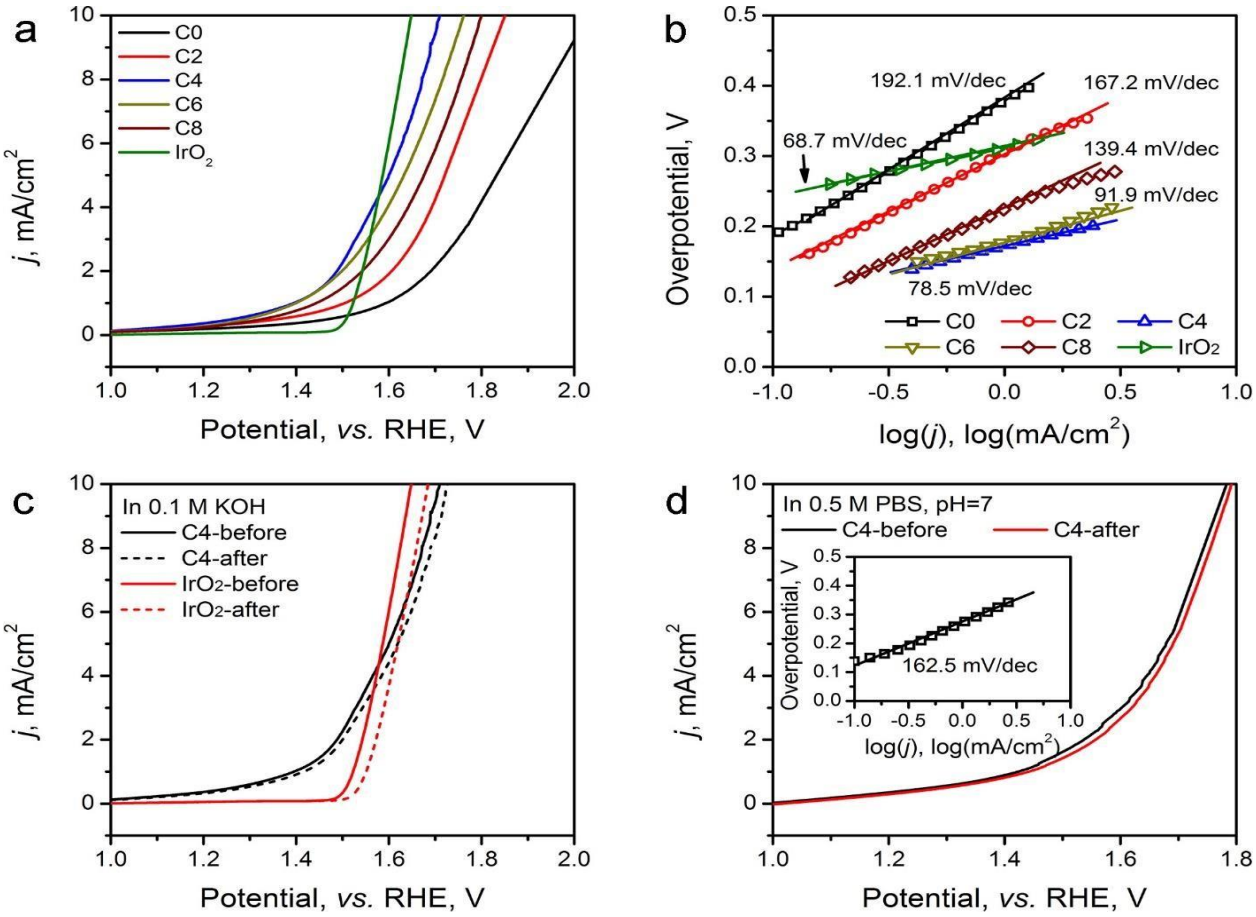


**Figure 12**. OER performance of various carbon electrocatalysts. (a) LSV scan and (b) Tafel plots of various electrocatalysts in in 0.1 M KOH electrolyte. (c) LSV curves of the C4 electrocatalysts before and after 2000 CV cycles between 1.2 to 1.8 V (vs. RHE, scan te=50mV/s) in 0.1 M KOH. (d) LSV

curves of the C4 electrocatalysts before and after 2000 CV cycles between 1.2 to 1.8 V (vs. RHE, scan rate=50mV/s) in 0.5 M PBS electrolyte (pH=7), inset: Tafel plot of C4 electrocatalyst in PBS.

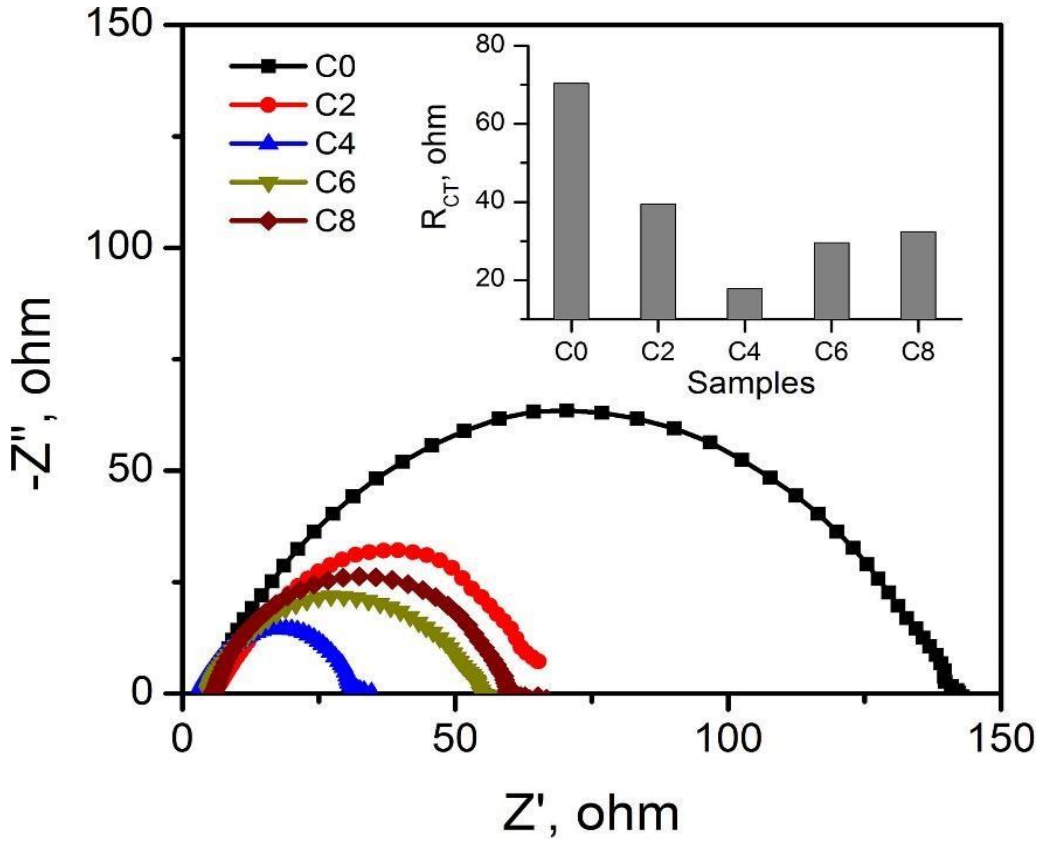


**Figure 13**. EIS Nyquist plot of various carbon electrocatalysts for OER. All plots are recorded with an overpotential of 0.4 V. Inset: fitted polarization resistance (RCT) values of C0~C8 samples.

The porous structure of the ZIF-8-derived carbon electrocatalysts can improve the mass transportation of ions in the electrolyte and gases generated [70]. Such effectiveness has been demonstrated by measuring the OER performance of the optimal ZIF-8-C4 at the different LSV scan rates from 5 to 100 mV/s. As shown in Figure. 14, the observed current density is almost identical, indicating highly efficient mass transportation [70].

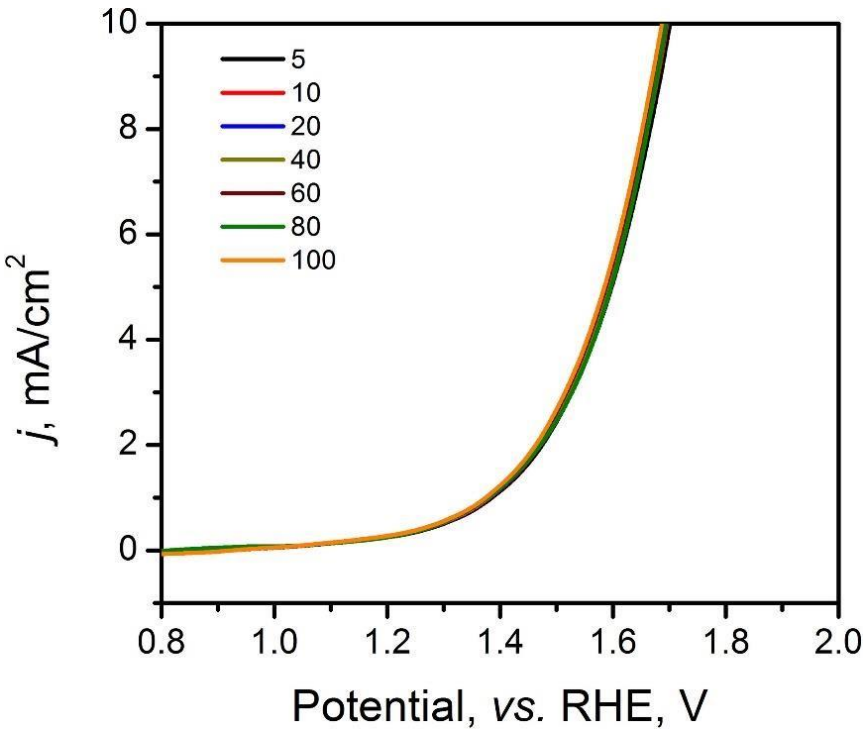


**Figure 14**. OER LSV curve of C4 sample obtained at different scan rate in 0.1 M KOH electrolyte.

I further compared the durability of OER electrocatalytic activity of ZIF-8-C4 with the commercial $IrO_2$ catalyst in 0.1 M KOH electrolyte by CV cycling and chronoamperometric tests. The results given in Figure. 12c show that after 2000 CV cycles from 1.2 to 1.8 V (*vs.* RHE), ZIF-8-C4 has an increment of 16 mV in its $\eta_{10}$, which is much smaller than that of $IrO_2$ at 52 mV. The chronoamperometric test (see Figure. 15) performed in 0.1 M KOH at 10 mA/cm$^2$ for 10 h yielded similar results. The overpotential required by ZIF-8-C4 increases by ~6.8% after 10 hours, while the overpotential required by $IrO_2$ increases by ~15.1%. Last, Figure. 12d shows that ZIF-8-C4 also has a reasonable good electrocatalytic activity and cycling stability in the neutral 0.5 M PBS buffer (pH=7), suggesting the possible application of ZIF-8-C4 for water splitting in neutral electrolytes. Meanwhile, to further assess C4 electrocatalyst practical use, the performance of C4 sample is compared with recent metal-free electrocatalysts in 0.1 M KOH in Table A5. Compared with other metal-free electrocatalysts, C4 shows good performance. Therefore, the results for the OER reactions suggest that C4 could be an active electrocatalyst for oxygen evolution reaction.

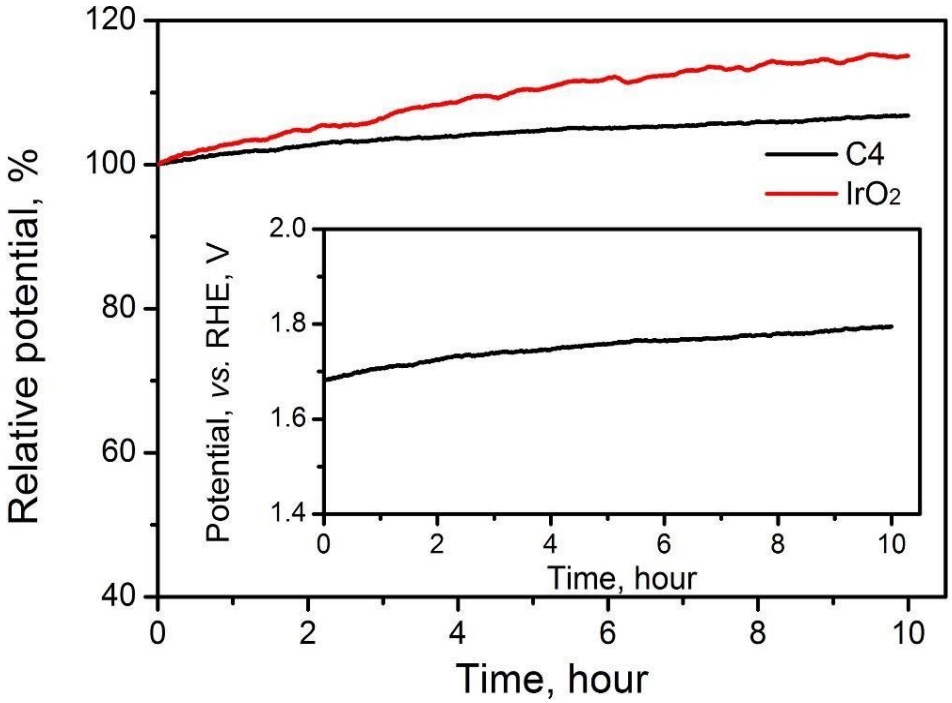


**Figure 15**. OER chornoampermetric test of the C4 sample performed at 10 mA/cm2 in 0.1 M KOH electrolyte.

### 3.5 Correlation between HER/OER activity and cathodic polarization treatment duration

The above catalytic performance evaluations show an obvious correlation between the HER/OER activity and the cathodic polarization treatment duration. I explored the possible role of the surface area, pore size distribution, and surface functionality changes of carbon materials induced by the cathodic polarization treatment. First, I examined the changes in surface area. The electrochemical active surface area (ECSA) of various ZIF-8-derived carbon electrocatalysts were determined and the results are shown in Table 1 and Figure. 4. The cathodic activation induced minor decreases in the ECSA of the ZIF-8-derived carbon electrocatalysts. Comparing with the 785.7 $m^2/g$ of ZIF-8-C0, the ZIF-8-C4 and ZIF-8-C6 retained the large ECSA of 740.5 and 706.0 $m^2/g$, respectively. Second, Figure. 2 shows that the pore size distributions of the carbon electrocatalysts are almost identical. Thus, I concluded that the surface area and pore size distribution are not the major contributing factors for the observed correlation. Next, I examined whether the correlation originates from the changes in N- and O-containing surface functional groups. Such functional groups have been found to cause variations in surface charge density of carbons and strongly influenced the electrochemical activity of carbon

materials [73, 74]. As shown in Figure. 16a, the two HER performance parameters, namely the $\eta_{10}$ and Tafel slope, are plotted against the abundance changes of several O and N functionalities calculated from XPS analysis (see Table A1 and A2 in Appendix). Oxidized N and carboxylic O have been proposed as active sites in carbon electrocatalysts for HER. Figure. 16a shows that HER performance gets better with the increase of these two functional groups. However, oxidized N is decreased and carboxylic O is increased after 4 hours treatment. It is due to that cathodic polarization mainly results in an increase of the carboxylic C and a decrease of acidic groups (Oxidized N) during cathodic pretreatment at -2.0 V. [56] ZIF-8-C6 having the high concentration of these active sites shows the highest catalytic activity. Extending the treatment duration to 8 hours could further increase the abundance of carboxylic O. According to mechanism, cathodic treatment could mainly promote hydrogen ions to change surface of the carbon materials by being charged with negative potential and then generate oxygenated functional groups. Therefore, with treatment time increasing, the surface of carbon has more time react with hydrogen ions, and final create more oxygenated functional groups, for instance, oxidized-N and C=O etc. Such oxidized-N and C=O play the part of $H^+$ acceptors or protons, which are benefit for $H_2$ formation and further enhance the HER and OER performance. However, the increased $I_D/I_G$ ratio observed in its Raman spectrum suggests more defective sites and more severe structural damages in the graphitic carbon framework (Figure. 3), which leads to reduced electrical conductivity (Figure. 13). In accordance, the HER performance of ZIF-8-C8 turned out to be poorer.

Recent experimental and theoretical studies have shown that p-type doping sites, such as pyridinic N and ketonic O, are responsible for the OER catalytic activity because these functional groups can withdraw electrons from adjacent C atoms to facilitate the adsorption of $OH^-$ and $OOH^-$ intermediates [75]. Figure. 16b shows that the OER performance has a strong connection with the abundances of pyridinic N and ketonic O. ZIF-8-C4 has the highest abundance of ketonic O (4.05 at.%) and pyridinic N (1.35 at.%) among the five ZIF-8-derived carbon electrocatalysts, which leads to the optimal OER

electrocatalytic activity. Further extending the treatment duration results in the reduction of these active sites, and lowers the OER performance. Overall, Figure. 16 confirmed that the changes in N- and O-containing surface functional groups induced by the cathodic polarization treatment is the main reason for the observed improvment in HER/OER activity.

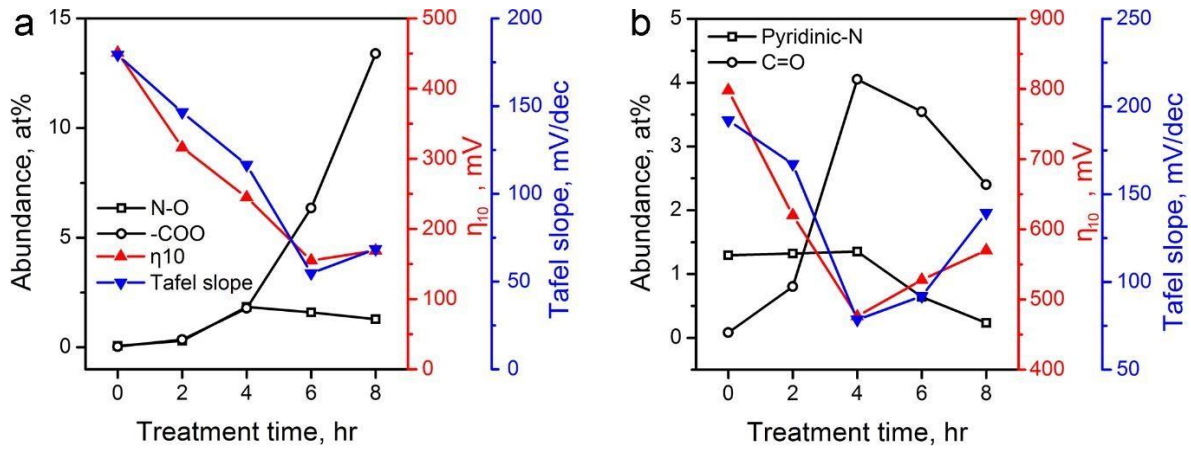


**Figure 16**. The corrections between the abundance of several major functional groups on ZIF-8-derived carbon electrocatalysts and their electrocatalytic performances for (a) HER (oxidized N and carboxylic O), and (b) OER (pyridinic N and ketonic O). The abundance of these functional groups (Table A2) was calculated using data in Table A1. Electrocatalytic performances of η10 and Tafel slopes were extracted from Figure. 10 and 12.

### 3.6 Contact angle measurement of C0~C8 electrocatalysts.

Improved surface wettability through cathodic treatment can also profit for electrocatalytic performance because improved wetness of the carbon surface can enhance interactions between the electrolyte and surface active sites. The contact angle of various carbon electrocatalysts have been measured from electrocatalyst thin film deposited on flat glass slides. The contact angle of various dry carbon electrocatalysts have decreased from 88.4 ° of C0 sample, to 67.6° of C4 sample, 58.8° of C6 and 44.5° of C8 sample (Figure 17), stating after surface chemistry modulation by cathodic treatment, the surface wettability had progressive improvement. Overall, it has been demonstrated that cathodic

treatment is an effective method to modulate carbon surface chemistry, and feasible for synthesizing efficient carbon electrocatalysts.

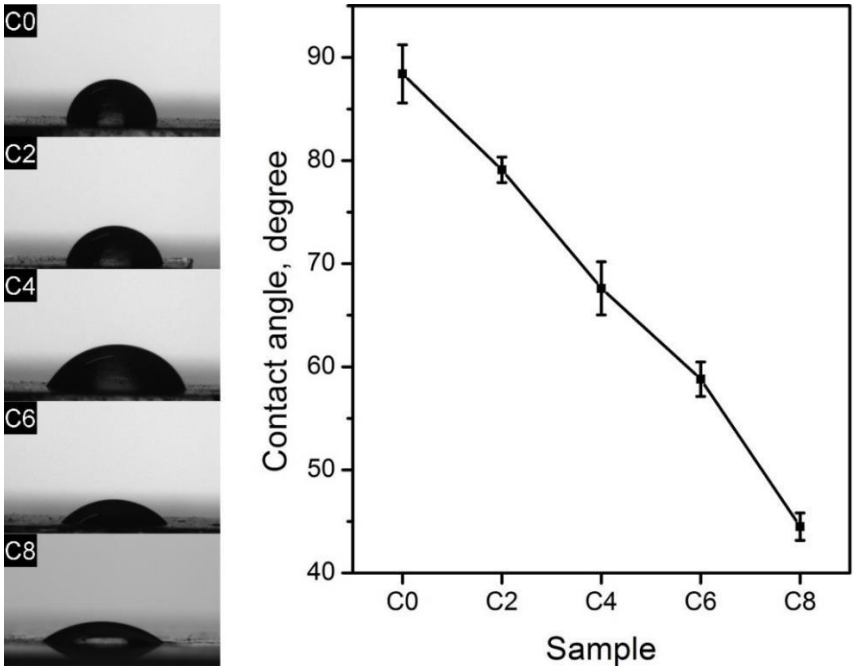


**Figure 17**. Contact angle measurement of C0~C8 electrocatalysts.

### 3.7 Total water splitting using optimal carbon electrocatalysts

To further demonstrate the capability of the carbon electrocatalysts for efficient total water splitting, I have fabricated a two-electrode water electrolyzer using ZIF-8-C6 in the cathode (for HER), and ZIF8-C4 in the anode (for OER) in 0.1 M KOH electrolyte (see the photo in Figure. 18a). For this demonstration, I have drop cast ZIF-8-C4 and ZIF-8-C6 on separate pieces of carbon clothes (1 × 1 $cm^2$ each) with the areal mass loading of 0.5 $mg/cm^2$. Figure. 18b shows that the assembled electrolyzer can steadily work at the current density of 10 $mA/cm^2$ over 8 hours at the potential of 1.82 V. Abundant $H_2$ and $O_2$ bubbles were observed on the electrode surface, and they dissipated in the electrolyte quickly. The amount of the produced $O_2$ and $H_2$ was quantified periodically, and the gas production was observed to be steady over 8 hours as seen in Figure. 18c. Crucially, the Faradaic efficiency of the water electrolyzer can reach up to 97.8% after an 8-hour test, which is highly promising for practical applications.

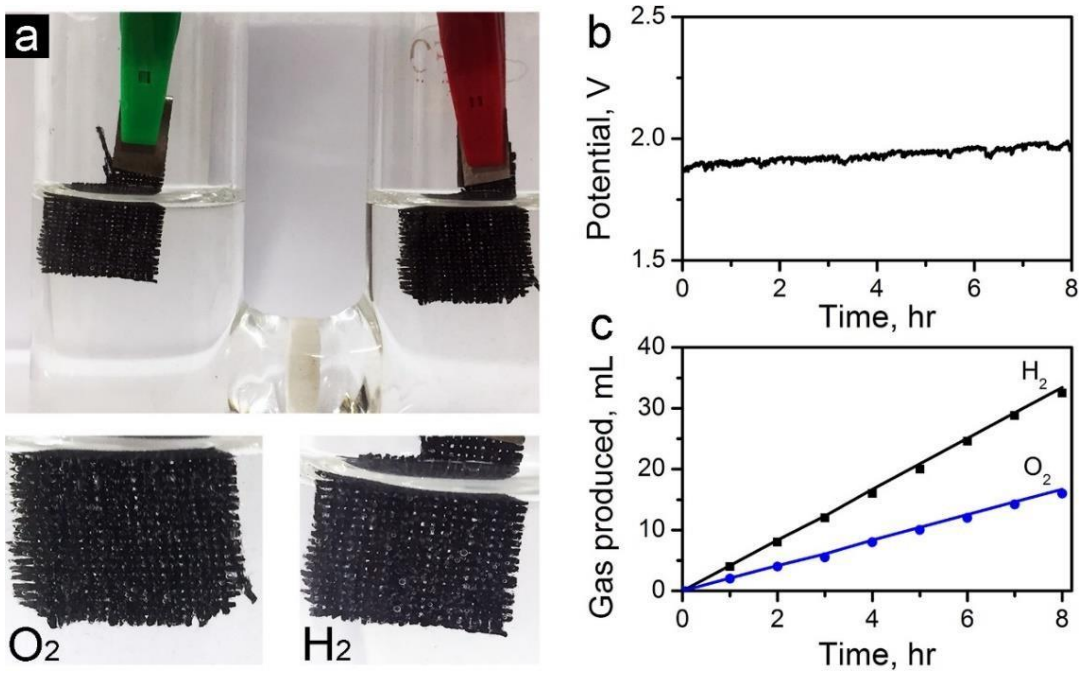


**Figure 18**. Total water splitting performance of C4 and C6 electrocatalysts in 0.1 M KOH (a) Photograph of a full-water splitter built up using C4 and C6 electrocatalysts as anode and cathode (b) Water splitting performance recorded at 10 mA/cm2 for 8 hours. (c) The amount of H2 and O2 produced from this electrolyser in comparison with theoretical values.

# 4. Conclusion

In summary, I have developed a simple but efficient method to obtain the surface chemical modulated metal free carbon materials which have excellent water splitting performance. By controlling the time of cathodic activation applied on the MOF-derived carbon electrocatalysts in 0.5 M $H_2SO_4$, strong correlation between treatment time and type and abundance of surface functional groups as well as their electrocatalytic performance of the modulated carbon electrocatalysts has been unveiled. I have confirmed that after 6 hours and 4 hours cathodic treatment, the optimal samples with superior HER or OER performance can be obtained, respectively. Using the C6 and C4 as cathode and anode, a two electrode electrolyser can deliver hydrogen and oxygen with nearly 100% efficiency. Hence, a novel and effective strategy to activate the surface chemical structure of carbon electrocatalysts has been demonstrated, which can result in a new discovery of producing a carbon electrocatalyst with excellent performance. Additionally, as a general electrode treatment method, cathodic polarization, can be extended to other elements/materials to improve their electro-catalytic performance.

# 5. Reference

[1] M.G. Walter, E.L. Warren, J.R. McKone, S.W. Boettcher, Q. Mi, E.A. Santori, N.S. Lewis, Chem. Rev. 110 (2010) 6446-6473.

[2] M. Götz, J. Lefebvre, F. Mörs, A. McDaniel Koch, F. Graf, S. Bajohr, R. Reimert, T. Kolb, Renew. Energy 85 (2016) 1371-1390.

[3] H. Dau, C. Limberg, T. Reier, M. Risch, S. Roggan, P. Strasser, Chemcatchem 2 (2010) 724-761.

[4] I.C. Man, H.Y. Su, F. Calle-Vallejo, H.A. Hansen, J.I. Martinez, N.G. Inoglu, J. Kitchin, T.F. Jaramillo, J.K. Norskov, J. Rossmeisl, Chemcatchem 3 (2011) 1159-1165.

[5] C.C.L. McCrory, S. Jung, J.C. Peters, T.F. Jaramillo, J. Am. Chem. Soc. 135 (2013) 16977-16987.

[6] S.H. Joo, S.J. Choi, I. Oh, J. Kwak, Z. Liu, O. Terasaki, R. Ryoo, Nature 412 (2001) 169-172.

[7] S.A. Grigoriev, P. Millet, V.N. Fateev, J. Power Sources 177 (2008) 281-285.

[8] Y. Liang, Y. Li, H. Wang, H. Dai, J. Am. Chem. Soc. 135 (2013) 2013-2036.

[9] C. Hu, L. Dai, Angew. Chem. Int. Ed. 55 (2016) 11736-11758.

[10] J. Zhang, Z. Zhao, Z. Xia, L. Dai, Nat. Nano. 10 (2015) 444-452.

[11] W. Zhou, J. Jia, J. Lu, L. Yang, D. Hou, G. Li, S. Chen, Nano Energy 28 (2016) 29-43. [12] G. Wu, A. Santandreu, W. Kellogg, S. Gupta, O. Ogoke, H. Zhang, H.-L. Wang, L. Dai, Nano Energy 29 (2016) 83-110.

[13] Y. Zheng, Y. Jiao, L.H. Li, T. Xing, Y. Chen, M. Jaroniec, S.Z. Qiao, ACS Nano 8 (2014) 5290-5296.

[14] C. Hu, L. Dai, Adv. Mater. 29 (2017) 1604942.

[15] X. Lu, W.-L. Yim, B.H.R. Suryanto, C. Zhao, J. Am. Chem. Soc. 137 (2015) 2901-2907.

[16] A. Mulyadi, Z. Zhang, M. Dutzer, W. Liu, Y. Deng, Nano Energy 32 (2017) 336-346.

[17] Y. Zheng, Y. Jiao, Y. Zhu, L.H. Li, Y. Han, Y. Chen, A. Du, M. Jaroniec, S.Z. Qiao, Nat. Commun. 5 (2014) 3783.

[18] H.B. Yang, J. Miao, S.F. Hung, J. Chen, H.B. Tao, X. Wang, L. Zhang, R. Chen, J. Gao, H.M.

Chen, L. Dai, B. Liu, Sci. Adv. 2 (2016) e1501122.

[19] J. Zhang, L. Qu, G. Shi, J. Liu, J. Chen, L. Dai, Angew. Chem. 128 (2016) 2270-2274.

[20] T.Y. Ma, S. Dai, M. Jaroniec, S.Z. Qiao, Angew. Chem. Int. Ed. 53 (2014) 7281-7285.

[21] T.Y. Ma, J. Ran, S. Dai, M. Jaroniec, S.Z. Qiao, Angew. Chem. Int. Ed. 54 (2015) 4646-4650.

[22] G.-L. Tian, Q. Zhang, B. Zhang, Y.-G. Jin, J.-Q. Huang, D.S. Su, F. Wei, Adv. Funct. Mater. 24

(2014) 5956-5961.

[23] R. Li, Z. Wei, X. Gou, ACS Catalysis 5 (2015) 4133-4142.

[24] J. Duan, S. Chen, M. Jaroniec, S.Z. Qiao, ACS Nano 9 (2015) 931-940.

[25] Wu, J.; Pisula, W.; Müllen, K. Chem. Rev. 2007, 107, 718−747.

[26] Stoller, M. D.; Park, S.; Zhu, Y.; An, J.; Ruoff, R. S. Nano Lett. 2008, 8, 3498−3502.

[27] Sahoo, N. G.; Pan, Y.; Li, L.; Chan, S. H. Adv. Mater. 2012, 24, 4203−4210.

[28] P. Wu, Z. W. Cai, Y. Gao, H. Zhang and C. X. Cai, Chem. Commun., 2011, 47, 11327–11329.

[29] P. Wu, Y. D. Qian, P. Du, H. Zhang and C. X. Cai, J. Mater. Chem., 2012, 22, 6402–6412.

[30] Y. H. S. Park, J. O. Hwang, E.-S. Lee, L. B. Casabianca, W. Cai, J. R. Potts, H.-W. Ha, S. Chen, J. Oh, S. O. Kim, Y.-H. Kim, Y. Ishii and R. S. Ruoff, Nat. Commun., 2012, 3, 1–8.

[31] D. H. Long, W. Li, L. C. Ling, J. Miyawaki, I. Mochida and S. H. Yoon, Langmuir, 2010, 26, 16096–16102.

[32] B. Jiang, C. Tian, L. Wang, L. Sun, C. Chen, X. Nong, Y. Qiao and H. Fu, Appl. Surf. Sci., 2012, 258, 3438–3443.

[33] L. Sun, L. Wang, C. G. Tian, T. X. Tan, Y. Xie, K. Y. Shi, M. T. Li and H. G. Fu, RSC Adv., 2012, 2, 4498–4506.

[34] J. W. Lee, J. M. Ko and J. D. Kim, Electrochim. Acta, 2012, 85, 459–466.

[35] Y. J. Zhang, K. Fugane, T. Mori, L. Niu and J. H. Ye, J. Mater. Chem., 2012, 22, 6575–6580.

[36] Y. Z. Chang, G. Y. Han, J. P. Yuan, D. Y. Fu, F. F. Liu and S. D. A. Li, J. Power Sources, 2013,

238, 492–500.

[37] Dai, L.; Xue, Y.; Qu, L.; Choi, H. J.; Baek, J. B. Chem. Rev. 2015, 115, 4823−4892.

[38] Li, Q.; Mahmood, N.; Zhu, J.; Hou, Y.; Sun, S. Nano Today 2014, 9, 668−683.

[39] Wang, X.; Sun, G.; Routh, P.; Kim, D. H.; Huang, W.; Chen, P. Chem. Soc. Rev. 2014, 43, 7067−7098.

[40] Kong, X. K.; Chen, C. L.; Chen, Q. W. Chem. Soc. Rev. 2014, 43, 2841−2857.

[41] N. Holmberg and K. Laasonen, J. Phys. Chem. Lett., 2015, 6, 3956.

[42] N. Holmberg and K. Laasonen, J. Phys. Chem. C, 2015, 119, 16166.

[43] S. Chen, J. Duan, M. Jaroniec and S.-Z. Qiao, Adv. Mater., 2014, 26, 2925.

[44] Y. Zheng, Y. Jiao, Y. Zhu, L. H. Li, Y. Han, Y. Chen, A. Du, M. Jaroniec and S. Z. Qiao, Nat. Commun., 2014, 5, 3783.

[45] M. Shalom, S. Gimenez, F. Schipper, I. Herraiz-Cardona, J. Bisquert and M. Antonietti, Angew. Chem., Int. Ed., 2014, 53, 3654.

[44] L. Li, H. Yang, J. Miao, L. Zhang, H.-Y. Wang, Z. Zeng, W. Huang, X. Dong, B. Liu, ACS Energy Lett. (2017) 294-300.

[45] N. Cheng, Q. Liu, J. Tian, Y. Xue, A.M. Asiri, H. Jiang, Y. He, X. Sun, Chem. Commun. 51 (2015) 1616-1619.

[46] S. Yanagida, A. Kabumoto, K. Mizumoto, C. Pac and K. Yoshino, J. Chem. Soc., Chem. Commun., 1985, 474.

[47] R. S. Sprick, J.-X. Jiang, B. Bonillo, S. Ren, T. Ratvijitvech, P. Guiglion, M. A. Zwijnenburg, D. J. Adams and A. I. Cooper, J. Am. Chem. Soc., 2015, 137, 3265.

[48] 45 V. S. Vyas and B. V. Lotsch, Nature, 2015, 521, 41.

[49] Y. Zhao, R. Nakamura, K. Kamiya, S. Nakanishi and K. Hashimoto, Nat. Commun., 2013, 4, 2390.

[50] X. Yu, M. Zhang, J. Chen, Y. Li and G. Shi, Adv. Energy Mater., 2016, 6, 1501492.

[51] J. Zhang, Z. Zhao, Z. Xia and L. Dai, Nat. Nanotechnol., 2015, 10, 444.

[52] J. Lai, S. Li, F. Wu, M. Saqib, R. Luque and G. Xu, Energy Environ. Sci., 2016, 9, 1210.

[53] S. Ma, G. A. Goenaga, A. V. Call and D.-J. Liu, Chem.–Eur. J., 2011, 17, 2063–2067.

[54] T. Palaniselvam, B. P. Biswal, R. Banerjee and S. Kurungot, Chem.–Eur. J., 2013, 19, 9335–9342.

[55] L. Wei, H.E. Karahan, K. Goh, W. Jiang, D. Yu, Ö. Birer, R. Jiang, Y. Chen, J. Mater. Chem. A 3 (2015) 7210-7214.

[56] W. Cui, Q. Liu, N. Cheng, A.M. Asiri, X. Sun, Chem. Commun. 50 (2014) 9340-9342.

[57] Linjie Zhangb, Zixue Su c, Feilong Jiang a, Lingling Yang a, Jinjie Qian ab, Youfu Zhou a, Wenmu Li a and Maochun Hong. Nanoscale, 2014. 6, 6590-6602.

[58] Weijia Zhou, Jin Jia, Jia Lu, Linjing Yang, Dongman Hou, Guoqiang Li, Shaowei Chen. Nano Energy. 28(2016), 29-43.

[59] W Chaikittisilp, NL Torad, C Li, M Imura, N Suzuki, S Ishihara, K Ariga, Y Yamauchi. A European Journal, 2014, 20, 4217-4221.

[60] T. Asefa, Accounts of Chemical Research 49 (2016) 1873-1883.

[61] Z. Lin, G.H. Waller, Y. Liu, M. Liu, C.-p. Wong, Nano Energy 2 (2013) 241-248.

[62] K. Qu, Y. Zheng, S. Dai, S.Z. Qiao, Nano Energy 19 (2016) 373-381.

[63] R. Berenguer, J.P. Marco-Lozar, C. Quijada, D. Cazorla-Amorós, E. Morallon, Carbon 47 (2009) 1018-1027.

[64] R.K. Das, Y. Wang, S.V. Vasilyeva, E. Donoghue, I. Pucher, G. Kamenov, H.-P. Cheng, A.G. Rinzler, ACS Nano 8 (2014) 8447-8456.

[65] R. Chen, C. Yang, W. Cai, H.-Y. Wang, J. Miao, L. Zhang, S. Chen, B. Liu, Use of Platinum as the Counter Electrode to Study the Activity of Nonprecious Metal Catalysts for the Hydrogen Evolution Reaction, ACS Energy Lett. 2(5) (2017) 1070-1075.

[66] G. Dong, M. Fang, H. Wang, S. Yip, H.-Y. Cheung, F. Wang, C.-Y. Wong, S.T. Chu, J.C. Ho, Insight into the electrochemical activation of carbon-based cathodes for hydrogen evolution reaction, J. Mater. Chem. A 3(24) (2015) 13080-13086.

[67] S. Brunauer, L.S. Deming, W.E. Deming, E. Teller, On a theory of the van der Waals adsorption of gases, J. Am. Chem. Soc. 62(7) (1940) 1723-1732.

[68] R.R. Salunkhe, C. Young, J. Tang, T. Takei, Y. Ide, N. Kobayashi, Y. Yamauchi, A highperformance supercapacitor cell based on ZIF-8-derived nanoporous carbon using an organic electrolyte, Chem. Commun. 52(26) (2016) 4764-4767.

[69] W. Chaikittisilp, M. Hu, H. Wang, H.-S. Huang, T. Fujita, K.C.W. Wu, L.-C. Chen, Y. Yamauchi, K. Ariga, Nanoporous carbons through direct carbonization of a zeolitic imidazolate framework for supercapacitor electrodes, Chem. Commun. 48(58) (2012) 7259-7261.

[70] J.L. Figueiredo, M.F.R. Pereira, M.M.A. Freitas, J.J.M. Órfão, Modification of the surface chemistry of activated carbons, Carbon 37(9) (1999) 1379-1389.

[71] M.J. Matthews, M.A. Pimenta, G. Dresselhaus, M.S. Dresselhaus, M. Endo, Origin of dispersive effects of the Raman D band in carbon materials, Phys. Rev. B 59(10) (1999) R6585-R6588. [69] R. Berenguer, J.P. Marco-Lozar, C. Quijada, D. Cazorla-Amorós, E. Morallón, Effect of electrochemical treatments on the surface chemistry of activated carbon, Carbon 47(4) (2009) 10181027.

[70] S. Chen, J. Duan, M. Jaroniec, S.-Z. Qiao, Nitrogen and Oxygen Dual-Doped Carbon Hydrogel Film as a Substrate-Free Electrode for Highly Efficient Oxygen Evolution Reaction, Adv. Mater. 26(18) (2014) 2925-2930.

[71] Z. Lin, G.H. Waller, Y. Liu, M. Liu, C.-p. Wong, Simple preparation of nanoporous few-layer nitrogen-doped graphene for use as an efficient electrocatalyst for oxygen reduction and oxygen evolution reactions, Carbon 53 (2013) 130-136.

[72] J. Tian, Q. Liu, A.M. Asiri, K.A. Alamry, X. Sun, Ultrathin Graphitic C3N4 Nanosheets/Graphene

Composites: Efficient Organic Electrocatalyst for Oxygen Evolution Reaction, ChemSusChem 7(8) (2014) 2125-2130.

[73] J. Liang, Y. Jiao, M. Jaroniec, S.Z. Qiao, Sulfur and Nitrogen Dual-Doped Mesoporous Graphene Electrocatalyst for Oxygen Reduction with Synergistically Enhanced Performance, Angew. Chem. Int.

Ed. 51(46) (2012) 11496-11500.

[74] S. Gadipelli, T. Zhao, S.A. Shevlin, Z. Guo, Switching effective oxygen reduction and evolution performance by controlled graphitization of a cobalt-nitrogen-carbon framework system, Energy Environ. Sci. 9(5) (2016) 1661-1667.

[75] C.H. Choi, H.-K. Lim, M.W. Chung, J.C. Park, H. Shin, H. Kim, S.I. Woo, J. Am. Chem. Soc. 136(25) (2014) 9070-9077.

[76] Rahul R. Salunkhe, Christine Young, Jing Tang, Toshiaki Takei, Yusuke Ide, Naoya Kobayashi and Yusuke Yamauchi, Chemical Communications, 2016, 52, 4764, 10.1039/C6CC00413J

## Appendix

**Table A1**. Relative abundance of C, N and O in different bonding condition in C0~C8 samples calculated from high resolution XPS analysis.

| | | B.E., eV | Relative abundance, % | | | | |
|---|---|---|---|---|---|---|---|
| | | | C0 | C2 | C4 | C6 | C8 |
| C | $sp^2$-C | 283.4 | 75.65 | 73.51 | 72.6 | 71.19 | 64.36 |
| | Aryl-C | 284.8 | 12.95 | 10.82 | 7.95 | 6.22 | 9.81 |
| | C=O | 287.7 | 0.35 | 1.03 | 5.72 | 4.20 | 2.60 |
| | C-N/C-O | 286.2 | 8.56 | 10.82 | 6.12 | 4.92 | 2.60 |
| | O=C-O | 289.2 | 0.22 | 1.29 | 4.03 | 10.98 | 14.76 |
| | shakeup | 290.8 | 2.26 | 2.53 | 3.58 | 2.50 | 5.88 |
| N | Pyridinic- | 398.3 | 15.41 | 20.50 | 27.00 | 18.84 | 12.36 |
| | Pyrrolic- | 399.8 | 48.36 | 42.50 | 14.20 | 11.4 | 5.64 |
| | Graphitic- | 401.3 | 35.50 | 32.44 | 21.94 | 22.89 | 14.61 |
| | Oxidized- | 403.1 | 0.72 | 4.56 | 36.85 | 46.87 | 67.39 |
| O | -C=O | 530.8 | 10.25 | 26.34 | 47.39 | 27.06 | 12.92 |
| | C-O/-O- | 532.1 | 12.63 | 54.57 | 9.82 | 6.23 | 5.17 |
| | O=C-O | 533.3 | 4.69 | 11.58 | 20.84 | 48.48 | 72.00 |
| | NO | 534.6 | 2.48 | 2.04 | 18.34 | 13.96 | 6.34 |
| | Chemisorbed $H_2O$ | 536.7 | 69.95 | 5.47 | 3.62 | 4.27 | 3.58 |

**Table A2**. Absolute atomic abundance of C, N and O in different bonding condition in C0~C8 samples calculated from high resolution XPS analysis.

| | | B.E., eV | Abundance, at% | | | | |
|---|---|---|---|---|---|---|---|
| | | | C0 | C2 | C4 | C6 | C8 |
| C | $sp^2$-C | 283.4 | 68.693 | 66.53 | 62.76 | 59.44 | 50.52 |
| | Aryl-C | 284.8 | 11.763 | 9.79 | 6.87 | 5.19 | 7.70 |
| | C=O | 287.7 | 0.32 | 0.93 | 4.94 | 3.51 | 2.04 |
| | C-N/C-O | 286.2 | 7.78 | 9.79 | 5.29 | 4.11 | 2.04 |
| | O=C-O | 289.2 | 0.20 | 1.17 | 3.48 | 9.16 | 11.59 |
| | shakeup | 290.8 | 2.05 | 2.29 | 3.10 | 2.09 | 4.61 |
| N | Pyridinic- | 398.3 | 1.29 | 1.32 | 1.35 | 0.64 | 0.23 |
| | Pyrrolic- | 399.8 | 4.06 | 2.74 | 0.71 | 0.39 | 0.11 |
| | Graphitic- | 401.3 | 2.98 | 2.09 | 1.10 | 0.78 | 0.28 |
| | Oxidized- | 403.1 | 0.06 | 0.29 | 1.85 | 1.59 | 1.28 |
| O | -C=O | 530.8 | 0.08 | 0.80 | 4.05 | 3.54 | 2.40 |
| | C-O/-O- | 532.1 | 0.10 | 1.66 | 0.84 | 0.82 | 0.96 |
| | O=C-O | 533.3 | 0.04 | 0.35 | 1.78 | 6.35 | 13.39 |
| | NO | 534.6 | 0.02 | 0.06 | 1.57 | 1.83 | 1.18 |
| | Chemisorbed $H_2O$ | 536.7 | 0.56 | 0.17 | 0.31 | 0.56 | 0.67 |

**Table A3**. HER performance of metal-free carbon electrocatalysts in 0.5 M $H_2SO_4$.

| Carbon catalyst | Tafel slope, mV/dec | mV $\eta_{10}$, | loading, mg/cm$^2$ | $j_0$, mA/cm$^2$ | Ref. |
|---|---|---|---|---|---|
| C6 | 54.7 | 155 | 0.3 | $6.3 \times 10^{-2}$ | *This work* |
| N,P-graphene | 91.0 | 420 | 0.2 | $2.4 \times 10^{-4}$ | *ACS Nano* **2014**, *8*, 5290 |
| N,S-graphene | 81 | 276 | N/A | $8.4 \times 10^{-3}$ | Angew. Chemie. Int. Ed., **2015**, 54, 2131 |
| $C_3N_4$@NG | 51.5 | 240 | 0.1 | $3.5 \times 10^{-4}$ | Nat. Commun., **2014**, 5, 3783 |
| $C_3N_4$@G | 54 | 207 | 0.14 | $4.0 \times 10^{-2}$ | Angew. Chemie. Int. Ed., **2014**, 53, 13934 |
| C3N4@N-graphene-750 | 49.1 | 80 | N/A | $4.3 \times 10^{-1}$ | ACS Nano, **2015**, 9, 931 |
| p-MWCNT-aocp | 71.3 | N/A | N/A | $1.6 \times 10^{-3}$ | Chem. Commun., **2014**, 50, 9340 |
| N,S-carbon | 80.5 | 290 | N/A | N/A | Angew.Chem.Int.Ed., **2015**, 54 2131 |
| $C_{60}(OH)_8$ | 78 | N/A | 0.002 | $7 \times 10^{-4}$ | Angew. Chemie. Int. Ed., **2013**,52, 10867 |
| N-carbon | 109 | 239 | N/A | N/A | Sci.Rep., **2014**, 4, 7557 |
| N,P-bacteria carbon | 58.4 | 204 | 0.152 | $1.7 \times 10^{-2}$ | J. Mater. Chem. A, **2015**, 3, 7210 |
| B-carbon | 99 | 310 | N/A | N/A | Catal.Sci.Technol., **2014**, 4, 2023 |
| NSC/MPA-5 | 99 | 240 | 0.25 | $4.810^{-3}$ | Nano Energy, **2017**, 32, 336 |
| N,S-CNT | 67.8 | 120 | 0.285 | N/A | Nano Energy, **2015**, 16, |

| | | | | | |
|---|---|---|---|---|---|
| | | | | | 357 |
| N,S-carbon | 57.4 | 97 | 0.285 | N/A | J. Mater. Chem. A, **2015**, 3, 8840 |
| N,P-carbon | 79 | 213 | 0.2 | $2.43 \times 10^{-2}$ | J. Mater. Chem. A, **2015**, 3, 12642 |
| N-rich holey graphene (N-G) | 157 | 510 | 0.216 | $6.38 \times 10^{-3}$ | Nano Energy, **2015**, 15, 567 |
| $C_3N_4$@S,Se-G | 86 | 300 | 0.283 | $6.27 \times 10^{-3}$ | J. Mater. Chem. A, **2015**, 3, 12810 |

**Table A4**. HER performance comparison with recent metal-free carbon electrocatalysts in 0.1 M KOH.

| Carbon catalyst | Tafel slope, mV/dec | $\eta_{10}$, mV | Ref. |
|---|---|---|---|
| C6 | 97.4 | 336 | *This work* |
| SHG | 112 | 310 | Adv. Mater., **2017**, 29, 1604942 |
| N-rich holey graphene (N-G) | 157 | 510 | Nano Energy, **2015**, 15, 567 |
| N,P-G | N/A | >600 | ACS Nano, **2014**, 8, 5290 |
| N,P-C | N/A | 470 | Angew. Chem., **2016**, 128, 2270 |
| N,O,P-G | 154 | 450 | Energy Environ. Sci., **2016**, 9, 1210 |
| $C_3N_4$@N-G | N/A | >600 | Nat. Commun., **2014**, 5, 3783 |
| $C_3N_4$@S,Se-G | 93 | 1100 | J. Mater. Chem. A, **2015**, 3, 12810 |
| $C_3N_4$@N,P-G | 129 | 580 | ChemCatChem, **2015**, 7, 3873 |

**Table A5**. OER performance comparison with recent metal-free carbon electrocatalysts in 0.1 M KOH.

| Carbon catalyst | Electrolyte | Tafel slope, mV/dec | $\eta_{10}$, mV | Ref. |
|---|---|---|---|---|
| C4 | 0.1 M KOH | 78.5 | 476 | *This work* |
| SHG | 0.1 M KOH | 71 | 370 | Adv. Mater., **2017**, 29, 1604942 |
| N-carbon film | 0.1 M KOH | 128 | 190 | Adv. Sci., **2015**, 2, 1400015 |
| N-doped CNT | 0.1 M KOH | 383 | 450 | ACS Appl. Mater. Interfaces, **2015**, 7, 11991 |
| N-doped graphite | 0.1 M KOH | N/A | 380 | Nat. Comm., **2013**, 4, 2390 |
| N-doped carbon | 0.1 M KOH | N/A | 390 | Carbon, **2013**, 53, 130 |
| Oxidized carbon cloth | 0.1 M KOH | 82 | 490 | Chem. Comm., **2015**, 51, 1616 |
| N,P-graphene | 0.1 M KOH | 70 | 340 | ACS Catal., **2015**, 5, 4133 |
| N,O-carbon hydrogel | 0.1 M KOH | 141 | 400 | Adv. Mater., **2014**, 26, 2925 |
| N,P-G | 0.1 M KOH | 59 | 420 | Nano Energy, **2016**, 19, 373 |
| N,O,P-G | 0.1 M KOH | 84 | 400 | Energy Environ. Sci., **2016**, 9, 1210 |
| g-$C_3N_4$/G | 0.1 M KOH | 68.5 | 580 | ChemSusChem, **2014**, 7, 2125 |
| N-G/CNT | 0.1 M KOH | 97 | 510 | Small, **2014**, 10, 2251 |
| N-GRW | 0.1 M KOH | 62 | 440 | Sci. Adv., **2016**, 2, e1501122 |

| | | | | |
|---|---|---|---|---|
| Surface oxidized MWCNT | 0.1 M KOH | 72 | 450 | J. Am. Chem. Soc, **2015**, 137, 2901 |
| P-$C_3N_4$ | 0.1 M KOH | 61.6 | 400 | Angew. Chem, Int. Ed., **2015**, 54, 4650 |
| g-$C_3N_4$-CNT | 0.1 M KOH | 83 | 350 | Angew. Chem. Int. Ed., **2014**, 53, 7281 |
| N-Carbon nanocable | 0.1 M KOH | | 520 | Adv. Funct. Mater., **2014**, 24, 5956 |